Ready-to-use Fourier domain templates for compact binaries inspiraling along moderately eccentric orbits

Srishti Tiwari,[1,*] Achamveedu Gopakumar,[1] Maria Haney,[2] and Phurailatapam Hemantakumar[3]
[1]Department of Astronomy and Astrophysics, Tata Institute of Fundamental Research, Mumbai 400005, India
[2]Physik-Institut, Universität Zürich, Winterthurerstrasse 190, 8057 Zürich, Switzerland
[3]Indian Institute of Technology, Mumbai 400076, India

(Received 13 March 2019; published 10 June 2019)

We derive analytic expressions that provide the Fourier domain gravitational wave (GW) response function for compact binaries inspiraling along moderately eccentric orbits. These expressions include amplitude corrections to the two GW polarization states that are accurate to the first post-Newtonian (PN) order. Additionally, our fully third post-Newtonian (3PN)-accurate GW phase evolution incorporates eccentricity effects up to sixth order at each PN order. Further, we develop a prescription to incorporate analytically the effects of the 3PN-accurate periastron advance in the GW phase evolution. This is how we provide a ready-to-use and efficient inspiral template family for compact binaries in moderately eccentric orbits. Preliminary GW data analysis explorations suggest that our template family should be required to construct analytic inspiral-merger-ringdown templates to model moderately eccentric compact binary coalescence.

DOI: 10.1103/PhysRevD.99.124008

I. INTRODUCTION

Observations of gravitational wave (GW) events by the advanced LIGO and VIRGO GW interferometers are ushering in the era of GW astronomy [1,2]. These GW events include merging black hole (BH) binaries and an inspiraling neutron star (NS) binary [3–9]. Several scenarios that include long-lived (galactic) field binaries, star clusters, galactic nuclei, and active galactic nuclei can produce these observed GW events [10–14]. Fortunately, it may be possible to extract valuable information about the astrophysical origins of GW events in the near future. This requires accurate GW measurements of the spin-orbit misalignment or the orbital eccentricities of these GW events [15–17]. Using both frequency and time-domain inspiral-merger-ringdown (IMR) waveforms, residual orbital eccentricities of the first two GW events were restricted to be below 0.15 when these binaries entered the aLIGO frequency window [18,19]. Strictly speaking, the so far detected GW events do not exhibit any observational signatures of residual orbital eccentricities and are faithfully captured by IMR templates associated with compact binaries merging along quasicircular orbits.

However, there exists a number of astrophysical scenarios that can produce GW events with non-negligible eccentricities in the frequency windows of ground-based GW detectors. Dense star clusters like the ubiquitous globular clusters are the most promising sites to form aLIGO relevant compact binaries with non-negligible orbital eccentricities [20]. A recent realistic modeling of globular clusters that involve general relativistic few body interactions provided a non-negligible fraction of BH binaries with eccentricities >0.1 as they enter the aLIGO frequency window [14,21–25]. Additionally, there exists a number of other astrophysical scenarios that can force stellar mass compact binaries to merge with orbital eccentricities. This includes a GW induced merger during hyperbolic encounters between BHs in dense clusters [26] and mergers influenced by the Kozai effect in few body systems as explored in many detailed investigations (see Ref. [27] and references therein). Further, a very recent investigation pointed out that less frequent binary-binary encounters in dense star clusters can easily produce eccentric compact binary coalescence [28]. These detailed investigations suggest that it may be reasonable to expect GW events with non-negligible orbital eccentricities in the coming years. Non-negligible orbital eccentricities may be helpful to improve the accuracy with a network of GW interferometers to constrain parameters of compact binary mergers [29,30]. Moreover, massive BH binaries in eccentric orbits are of definite interest to maturing pulsar timing arrays and the planned Laser Interferometer Space Antenna (LISA) [31,32].

There are different ongoing investigations to model eccentric compact binary coalescence. These efforts aim to provide template families that model GWs from IMR phases of eccentric coalescence. The initial effort, detailed in Ref. [19], provided a time-domain IMR family that requires orbital eccentricity to be negligible during the merger phase.

*srishti.tiwari@tifr.res.in

The inspiral part of the above waveform family was based on a certain x model, introduced in Ref. [33], that adapted the GW phasing formalism of Refs. [34,35]. Additionally, a preliminary comparison with two numerical relativity (NR) waveforms was also pursued in Ref. [19]. An improved version of the above family was presented in Ref. [36] that employed certain quasicircular merger waveform and which can reproduce their NR simulations for any mass ratio below 4. These waveform families are expected to model GWs from eccentric coalescence when initial eccentricities were usually below 0.2. Very recently, another time-domain IMR family was introduced in Ref. [37]. This detailed effort combined various elements from post-Newtonian, self-force, and black hole perturbation approaches in tandem with NR simulations to model GWs from moderately eccentric nonspinning BH binary coalescence. The resulting IMR waveforms were validated with many NR simulations for eccentric binary BH mergers lasting around ten orbits with mass ratios below 5.5 and initial eccentricities below 0.2. The eccentric binary BH coalescence is also explored in the framework of the effective-one-body (EOB) approach [38]. A formalism to incorporate orbital eccentricity in the existing EOB approach to model quasicircular compact binary coalescence is presented in Ref. [39]. Additionally, Ref. [40] presented an EOB waveform family that incorporated elements of the second post-Newtonian (2PN)-accurate eccentric orbital description while comparing with few NR simulations for eccentric binary BH coalescence. In contrast, the LIGO Scientific Collaboration (LSC) adapted Ref. [41], which provided a crude IMR prescription to model GW signals from merging highly eccentric compact binaries. This was employed to probe the ability of few LSC algorithms to extract burstlike signals in the LIGO data [42]. Further, some of us developed a ready-to-use "effective eccentric variant" of the IMRPhenomD waveform to constrain the initial orbital eccentricity of the GW150914 black hole binary. This was pursued to justify the assumption of binary evolution along circular orbits for the event [18]. A crucial ingredient of the above IMR waveform family involved an eccentric version of the TaylorF2 approximant that incorporated in its Fourier phase the leading-order eccentricity corrections up to third post-Newtonian (3PN) order. The present paper provides fully analytic frequency domain interferometric response function $\tilde{h}(f)$ relevant for GW data analysis of nonspinning compact binaries inspiraling along moderately eccentric PN-accurate orbits.

Our computation is aimed at extending the widely used TaylorF2 approximant that provides analytic frequency domain GW templates for compact binaries inspiraling along quasicircular orbits [43]. This waveform family employs the method of stationary phase approximation (SPA) to compute analytically, the Fourier transform of temporally evolving GW polarization states, $h_\times$ and h_+, for quasicircular inspirals. The popular LSC approximant provides a fully analytic Fourier domain GW response function $\tilde{h}(f)$ that incorporates the 3.5PN-accurate Fourier phase [43]. In other words, this approximant provides general relativistic corrections to GW phase evolution that are accurate to $(v/c)^7$ order beyond the dominant quadrupolar order, where v is the orbital velocity. The present manuscript details our derivation of a fully analytic $\tilde{h}(f)$ with a 3PN-accurate Fourier phase with sixth order eccentricity contributions in terms of certain initial eccentricity at each PN order. Additionally, we include the first post-Newtonian (1PN)-accurate amplitude corrections and the effect of 3PN-accurate periastron advance on the Fourier phases.

To derive our eccentric approximant, we extend the postcircular scheme of Ref. [44] to higher PN orders. This scheme involves expanding the Newtonian accurate $h_\times$ and h_+ as a power series in orbital eccentricity that requires an analytic solution to the classic Kepler equation. We extend such a Newtonian approach by invoking a recent effort to solve analytically the PN-accurate Kepler equation in the small eccentricity limit [45]. This detailed computation also provided analytic 1PN-accurate amplitude-corrected expressions for $h_\times$ and h_+ as a sum over harmonics in certain mean anomaly l of PN-accurate Keplerian type parametric solution [45]. Additionally, the above PN-accurate decomposition explicitly incorporated the effect of the periastron advance on individual harmonics, numerically explored using a PN description in Ref. [46]. We combine such 1PN-accurate amplitude-corrected $h_\times$ and h_+ expressions that incorporated eccentricity contributions to sixth order at each PN order with the two beam pattern functions, $F_\times$ and F_+, to obtain a fully analytic time-domain GW response function $h(t)$. Our eccentric TaylorF2 approximant is obtained by applying the method of stationary phase approximation to such an analytic $h(t) = F_+ h_+ + F_\times h_\times$ expression.

To obtain analytic expressions for several Fourier phases at their associated stationary points of $h(t)$, we require additional PN-accurate expressions. This involves deriving the 3PN-accurate expression for the time eccentricity e_t, present in the 3PN-accurate Kepler equation [47], as a bivariate expansion in terms of orbital angular frequency ω, its initial value ω_0 and e_0, and the value of e_t at ω_0. This lengthy computation extends to the 3PN order, the idea of a certain *asymptotic eccentricity invariant* at the quadrupolar order, introduced in Ref. [48] and extended to 2PN in Ref. [49]. In fact, we adapted the approach of Ref. [49] by employing the appropriately modified 3PN-accurate $d\omega/dt$ and de_t/dt expressions of Refs. [50,51] to obtain the 3PN-accurate bivariate expression for e_t. A careful synthesis of the above listed PN-accurate expressions leads to a fully analytic frequency domain TaylorF2 approximant that included 1PN-accurate amplitude corrections and 3PN-accurate Fourier phases. An additional feature of our approximant is the inclusion of periastron advance effects to 3PN order. To explore the GW data analysis implications of these features, we perform preliminary *match* computations [52]. We conclude that the influences of the periastron advance are

non-negligible for moderately eccentric binaries, especially in the aLIGO frequency window. This observation should be relevant while constructing an IMR waveform family for compact binaries merging along moderate eccentric orbits.

This paper is structured as follows. In Sec. II, we summarize the efforts of Refs. [44,49] to obtain analytic $\tilde{h}(f)$ with the PN-accurate Fourier phase. The crucial inputs to construct our eccentric TaylorF2 approximant are also listed in this section. Our approach and crucial expressions to implement our eccentric approximant that incorporates eccentricity contributions up to $\mathcal{O}(e_t^6)$ to 3PN are presented in Sec. III. A brief summary and possible extensions are listed in Sec. IV while detailed expressions, accurate to $\mathcal{O}(e_0^4)$, are given in Appendix C.

II. POSTCIRCULAR EXTENSIONS TO CIRCULAR INSPIRAL TEMPLATES

We begin by reviewing two key efforts to include the effects of orbital eccentricity onto the circular inspiral templates [44,48]. This involves listing in Sec. II A the steps that are crucial to compute the analytic frequency domain GW response function with quadrupolar amplitudes and the PN-accurate Fourier phase in some detail. Various lengthy expressions, extracted from Refs. [45,50,51], are listed in Sec. II B, and will be crucial to compute the time-domain response function for eccentric binaries while incorporating effects of the periastron advance, higher-order radiation reaction, and amplitude corrections.

A. Quadrupolar-order $\tilde{h}(f)$ with PN-accurate Fourier phase

Following [53], we may express the GW interferometric response function as

$$h(t) = F_+(\theta_S,\phi_S,\psi_S)h_+(t) + F_\times(\theta_S,\phi_S,\psi_S)h_\times(t), \quad (2.1)$$

where $F_{\times,+}(\theta_S,\phi_S,\psi_S)$ are the two detector antenna patterns. These quantities depend on ϕ_S,θ_S, the right ascension and declination of the source, and a certain polarization angle ψ_S [53]. For eccentric inspirals, the explicit expressions for the quadrupolar-order GW polarization states, $h_\times$ and h_+, are given by Eqs. (3.1) of Ref. [44]. It is rather straightforward to express these Newtonian accurate expressions as a sum over harmonics in terms of the mean anomaly l. The resulting expressions read

$$h_{+,\times}(t) = -\frac{Gm\eta}{c^2 D_L} x \sum_{j=1}^{10} [C^{(j)}_{+,\times}\cos jl + S^{(j)}_{+,\times}\sin jl], \quad (2.2)$$

where D_L denotes the luminosity distance while the symmetric mass ratio η of a binary consisting of individual masses m_1 and m_2 is defined to be $\eta = (m_1 m_2)/m^2$ while the total mass $m = m_1 + m_2$. Further, we use the commonly used dimensionless PN expansion parameter $x = (\frac{Gm\omega}{c^3})^{2/3}$ where G, c, and ω are the gravitational constant, the speed of light in vacuum, and the orbital angular frequency, respectively. The Newtonian accurate amplitudes, $C^{(j)}_{+,\times}$ and $S^{(j)}_{+,\times}$, are written as a power series in orbital eccentricity e_t whose coefficients involve trigonometric functions of the two angles ι, β that specify the line of sight vector in a certain inertial frame. The derivation of these expressions is detailed in Ref. [44] and the required inputs are obtained by adapting a standard analytic approach to solve the classical Kepler equation in terms of the Bessel functions [54].

With the help of Eqs. (2.1) and (2.2), we obtain the interferometric strain for GWs from eccentric binaries as

$$h(t) = -\frac{Gm\eta}{c^2 D_L}\left(\frac{Gm\omega}{c^3}\right)^{2/3}\sum_{j=1}^{10}\alpha_j \cos(jl+\phi_j), \quad (2.3)$$

where $\alpha_j = \mathrm{sign}(\Gamma_j)\sqrt{\Gamma_j^2+\Sigma_j^2}$ and $\phi_j = \tan^{-1}(-\frac{\Sigma_j}{\Gamma_j})$. The two new functions, Γ_j and Σ_j, are defined as $\Gamma_j = F_+C^{(j)}_+ + F_\times C^{(j)}_\times$ and $\Sigma_j = F_+S^{(j)}_+ + F_\times S^{(j)}_\times$, respectively, as in Ref. [44]. We impose the effects of GW emission on the above strain by specifying how e_t and $\omega = 2\pi F$, with F being the orbital frequency, vary in time. In Ref. [44], the temporal evolutions of ω and e_t are governed by the following Newtonian (or quadrupolar) equations that were adapted from Refs. [55–57].

$$\frac{d\omega}{dt} = \frac{(Gm\omega)^{5/3}\omega^2\eta}{5c^5(1-e_t^2)^{7/2}}\{96+292{e_t}^2+37{e_t}^4\}, \quad (2.4a)$$

$$\frac{de_t}{dt} = -\frac{(Gm\omega)^{5/3}\omega\eta e_t}{15c^5(1-e_t^2)^{5/2}}\{304+121{e_t}^2\}. \quad (2.4b)$$

It is customary to solve these two coupled differential equations numerically to obtain $\omega(t)$ and $e_t(t)$ and hence temporally evolving $h(t)$. Interestingly, earlier efforts provided a certain analytic way for obtaining a temporal evolution for $\omega(t)$ and $e_t(t)$ that mainly involves the usage of hypergeometric functions [58–61].

However, it is possible to obtain an analytic frequency domain counterpart of the above $h(t)$ as demonstrated in Refs. [44,48]. This traditional approach involves the method of SPA, detailed in Ref. [62], to compute analytically the Fourier transform of $h(t)$. This was essentially demonstrated at the leading order in initial eccentricity e_0 in Ref. [48] and later extended to $\mathcal{O}(e_0^8)$ in Ref. [44]. Following Refs. [44,48], we write

$$\tilde{h}(f) = \tilde{\mathcal{A}}\left(\frac{Gm\pi f}{c^3}\right)^{-7/6}\sum_{j=1}^{10}\xi_j\left(\frac{j}{2}\right)^{2/3}e^{-i(\pi/4+\Psi_j)}, \quad (2.5)$$

where the overall amplitude $\tilde{\mathcal{A}}$ and the amplitudes of the Fourier coefficients ξ_j are given by

$$\tilde{\mathcal{A}} = -\left(\frac{5\eta\pi}{384}\right)^{1/2}\frac{G^2m^2}{c^5D_L}, \tag{2.6a}$$

$$\xi_j = \frac{(1-e_t^2)^{7/4}}{(1+\frac{73}{24}e_t^2+\frac{37}{96}e_t^4)^{1/2}}\alpha_j e^{-i\phi_j(f/j)}. \tag{2.6b}$$

In the approach of the stationary phase approximation, the crucial Fourier phase is given by

$$\Psi_j[F(t_0)] = 2\pi\int^{F(t_0)}\tau'\left(j-\frac{f}{F'}\right)dF', \tag{2.7}$$

where τ stands for $F/\dot{F}$. Note that one needs to evaluate the above integrals at appropriate stationary points t_0, defined by $F(t_0) = f/j$.

To obtain a fully analytic ready-to-use expression for $\tilde{h}(f)$, we need to follow few additional steps. Clearly, we require one to specify the frequency evolution of e_t with the help of Eqs. (2.4a) and (2.4b). The structure of these equations for $\dot{\omega}$ and $\dot{e}_t$ allows us to write $d\omega/de_t = \omega\kappa_N(e_t)$ and it turns out that κ_N depends only on e_t. This allows us to integrate analytically the resulting $d\omega/\omega = \kappa_N(e_t)de_t$ equation. The resulting expression can be written symbolically as $\omega/\omega_0 = \kappa'(e_t, e_0)$ where e_0 is the value of e_t at the initial ω value, namely, ω_0 [see Eq. (62) in Ref. [34] for the explicit form for $\kappa'(e_t, e_0)$]. Interestingly, one may invert such an expression in the limit $e_t \ll 1$ to obtain e_t in terms of e_0, ω, and ω_0 and it reads

$$e_t \sim e_0\chi^{-19/18} + \mathcal{O}(e_0^3), \tag{2.8}$$

where χ is defined as $\omega/\omega_0 = F/F_0$. We note that the above result was first obtained in Ref. [48] which influenced them to introduce the idea of an asymptotic eccentricity invariant. This relation allows us to write τ in terms of ω, ω_0 and e_0, as

$$\tau \sim \frac{5}{96\eta x^4}\left(\frac{Gm}{c^3}\right)\left[1-\frac{157e_0^2}{24}\chi^{-19/9}+\mathcal{O}(e_0^4)\right]. \tag{2.9}$$

It is now straightforward to compute analytically the indefinite integral for Ψ_j, namely,

$$2\pi\int\tau'\left(j-\frac{f}{F'}\right)dF' \tag{2.10}$$

which appears in Eq. (2.7) for $\tilde{h}(f)$. This leads to the following expression for Ψ_j, accurate to $\mathcal{O}(e_0^2)$ corrections:

$$\Psi_j \sim j\phi_c - 2\pi f t_c - \frac{3}{128\eta}\left(\frac{Gm\pi f}{c^3}\right)^{-5/3}\left(\frac{j}{2}\right)^{8/3} \times\left[1-\frac{2355e_0^2}{1462}\chi^{-19/9}+\mathcal{O}(e_0^4)\right], \tag{2.11}$$

where ϕ_c and t_c are the orbital phase at coalescence and the time of coalescence, respectively. Note that χ now stands for f/f_0 due to the use of the stationary phase condition. Additionally, we have rescaled $F_0 \to f_0/j$ to ensure that $e_t(f_0) = e_0$ while employing the above expression for e_t, given by Eq. (2.8). Indeed, our expression is consistent with Eq. (4.28) of Ref. [44] that employs the chirp mass to characterize the binary. A number of extensions to the above result is available in the literature. In fact, Ref. [44] computed the higher-order corrections to e_t in terms of e_0 up to $\mathcal{O}(e_0^7)$ and extended Ψ_j to $\mathcal{O}(e_0^8)$. Its PN extension, available in Ref. [49], provided 2PN corrections for Ψ_j that incorporated eccentricity corrections, accurate to $\mathcal{O}(e_0^6)$ at every PN order, while Ref. [63] computed 3PN-accurate Ψ_j that included leading-order e_0 contributions.

A crucial ingredient to such PN extensions is the derivation of the PN-accurate e_t expression in terms of e_0, χ, and x. In what follows, we summarize the steps that are required to obtain a 1PN-accurate expression for e_t (see Ref. [49] for details). The starting point of such a derivation is the 1PN-accurate differential equations for ω and e_t, obtainable from Eq. (3.12) in Ref. [49]. With these inputs, it is fairly straightforward to obtain the following 1PN-accurate expression for $d\omega/\omega$ that includes only the leading-order e_t contributions as

$$d\omega/\omega = \left\{-\frac{18}{19e_t}-\frac{3}{10108e_t}(-2833+5516\eta) \times\left(\frac{Gm\omega}{c^3}\right)^{2/3}\right\}de_t. \tag{2.12}$$

The fact that the ω term appears only at the 1PN order allows us to use the earlier derived Newtonian accurate $\omega = \omega_0(e_0/e_t)^{18/19}$ relation to replace ω on the right-hand side of the above equation. This leads to

$$d\omega/\omega \sim \left\{-\frac{18}{19e_t}-\frac{3}{10108}\left(\frac{e_0^{12/19}}{e_t^{31/19}}\right)(-2833+5516\eta)x_0\right\}de_t, \tag{2.13}$$

where $x_0 = (Gm\omega_0/c^3)^{2/3}$. We can integrate this equation to obtain $\ln\omega - \ln\omega_0$ in terms of e_t, e_0, and ω_0. The exponential of the resulting expression and its bivariate expansion in terms of x_0 and e_t result in

$$\omega \sim \left\{\left(\frac{e_0}{e_t}\right)^{18/19}+x_0\left(\frac{2833-5516}{2128}\eta\right) \times\left[\left(\frac{e_0}{e_t}\right)^{18/19}-\left(\frac{e_0}{e_t}\right)^{30/19}\right]\right\}\omega_0. \tag{2.14}$$

We invert the above equation to obtain e_t in terms of e_0 and x_0 after invoking the Newtonian accurate relation $e_t = e_0\chi^{-19/18}$ to replace the e_t terms associated with the x_0 term. This inversion and the associated bivariate expansion in terms of e_0 and x_0 require that $e_0 \ll 1$ and $x_0 \ll 1$. The resulting e_t expression reads

$$e_t \sim e_0\left\{\chi^{-19/18}+x_0\left(\frac{2833}{2016}-\frac{197}{72}\eta\right)(-\chi^{-7/18}+\chi^{-19/18})\right\}. \tag{2.15}$$

To obtain e_t as a bivariate expansion in terms of the regular PN parameter x and e_0, we employ the fact that $x/x_0=\chi^{2/3}$ and this results in

$$e_t \sim e_0\left\{\chi^{-19/18}+x\left(\frac{2833}{2016}-\frac{197}{72}\eta\right)(-\chi^{-19/18}+\chi^{-31/18})\right\}. \tag{2.16}$$

We are now in a position to obtain a 1PN-accurate Ψ_j expression that includes $\mathcal{O}(e_0^2)$ contributions both at the Newtonian and 1PN orders with the help of a 1PN-accurate $\tau=\omega/\dot{\omega}$ expression that is accurate to $\mathcal{O}(e_t^2)$ terms. A straightforward computation leads to the desired Ψ_j expression which reads

$$\begin{aligned}\Psi_j \sim{}& j\phi_c-2\pi f t_c-\left(\frac{3j}{256\eta}\right)x^{-5/2}\left\{1-\frac{2355e_0^2}{1462}\chi^{-19/9}\right.\\&+x\left[\frac{3715}{756}+\frac{55}{9}\eta+\left(\left[-\frac{2045665}{348096}-\frac{128365}{12432}\eta\right]\chi^{-19/9}\right.\right.\\&\left.\left.\left.+\left[-\frac{2223905}{491232}+\frac{154645}{17544}\eta\right]\chi^{-25/9}\right)e_0^2\right]\right\},\end{aligned} \tag{2.17}$$

where the quantities x and χ will have to be evaluated at the stationary point (see Ref. [49] for details). With the above equation, we explicitly listed our approach to compute PN-accurate Ψ_j that incorporates e_0 corrections at each PN order. In the present paper, we extend these computations to 3PN order while incorporating $\mathcal{O}(e_0^6)$ contributions at each PN order. These higher-order e_0 corrections are included as we desire to model GWs from moderately eccentric compact binary inspirals. In the next section, we provide crucial inputs that will be required to compute the analytic 1PN-accurate amplitude-corrected $\tilde{h}(f)$ with 3PN-accurate Fourier phases.

B. Analytic PN-accurate amplitude-corrected time-domain eccentric GW templates

The previous section showed that we require analytic expressions for the two GW polarization states as a sum over *harmonics* to construct the ready-to-use analytic $\tilde{h}(f)$. This influenced us to adapt Eqs. (44) and (45) in Ref. [45] that provided an analytic 1PN-accurate amplitude-corrected $h_{\times,+}(t)$ which additionally included the effects of the periastron advance on individual *harmonics*. This may be seen by a close inspection of appropriate terms in Eqs. (44), (45), (46), and (47) of Ref. [45]. To describe in detail how these improvements in GW polarization states change the harmonic structure of $h(t)$, we restrict our attention to quadrupolar-order contributions to $h_{\times,+}(t)$, given in Eqs. (44) and (45) of Ref. [45]. The explicit expressions for such "Newtonian" contributions to $h_{\times,+}(t)$ that include $\mathcal{O}(e_t^4)$ corrections read

$$\begin{aligned}h_\times^0 ={}& \frac{Gm\eta}{c^2D_L}x\left\{\cos(\phi+\phi')\left[\left(-3e_t+\frac{13e_t^3}{8}\right)c_i s_{2\beta}\right]+\sin(\phi+\phi')\left[\left(3e_t-\frac{13e_t^3}{8}\right)c_i c_{2\beta}\right]\right.\\&+\cos(2\phi)\left[\left(4-10e_t^2+\frac{23e_t^4}{4}\right)c_i s_{2\beta}\right]+\sin(2\phi)\left[\left(-4+10e_t^2-\frac{23e_t^4}{4}\right)c_i c_{2\beta}\right]\\&+\cos(3\phi-\phi')\left[\left(9e_t-\frac{171e_t^3}{8}\right)c_i s_{2\beta}\right]+\sin(3\phi-\phi')\left[\left(-9e_t+\frac{171e_t^3}{8}\right)c_i c_{2\beta}\right]\\&+\cos(4\phi-2\phi')[(16e_t^2-40e_t^4)c_i s_{2\beta}]+\sin(4\phi-2\phi')[(-16e_t^2+40e_t^4)c_i c_{2\beta}]\\&+\cos(5\phi-3\phi')\left[\frac{625}{24}e_t^3 c_i s_{2\beta}\right]+\sin(5\phi-3\phi')\left[\frac{-625}{24}e_t^3 c_i c_{2\beta}\right]+\cos(6\phi-4\phi')\left[\frac{81}{2}e_t^4 c_i s_{2\beta}\right]\\&+\sin(6\phi-4\phi')\left[\frac{-81}{2}e_t^4 c_i c_{2\beta}\right]+\cos(\phi-3\phi')\left[\frac{-7}{24}e_t^3 c_i s_{2\beta}\right]+\sin(\phi-3\phi')\left[\frac{-7}{24}e_t^3 c_i c_{2\beta}\right]\\&\left.+\cos(2\phi-4\phi')\left[-\frac{1}{4}e_t^4 c_i s_{2\beta}\right]+\sin(2\phi-4\phi')\left[-\frac{1}{4}e_t^4 c_i c_{2\beta}\right]\right\},\end{aligned} \tag{2.18}$$

$$
\begin{aligned}
h^0_+ = \frac{Gm\eta}{c^2 D_L} x \Bigg\{ & \cos(\phi+\phi')\left[\left(\frac{3e_t}{2}-\frac{13e_t^3}{16}\right)(1+c_i^2)c_{2\beta}\right] + \sin(\phi+\phi')\left[\left(\frac{3e_t}{2}-\frac{13e_t^3}{16}\right)(1+c_i^2)s_{2\beta}\right] \\
& + \cos(2\phi)\left[\left(-2+5e_t^2-\frac{23e_t^4}{8}\right)(1+c_i^2)c_{2\beta}\right] + \sin(2\phi)\left[\left(-2+5e_t^2-\frac{23e_t^4}{8}\right)(1+c_i^2)s_{2\beta}\right] \\
& + \cos(3\phi-\phi')\left[\left(-\frac{9e_t}{2}+\frac{171e_t^3}{16}\right)(1+c_i^2)c_{2\beta}\right] + \sin(3\phi-\phi')\left[\left(-\frac{9e_t}{2}+\frac{171e_t^3}{16}\right)(1+c_i^2)s_{2\beta}\right] \\
& + \cos(4\phi-2\phi')[(-8e_t^2+20e_t^4)(1+c_i^2)c_{2\beta}] + \sin(4\phi-2\phi')[(-8e_t^2+20e_t^4)(1+c_i^2)s_{2\beta}] \\
& + \cos(5\phi-3\phi')\left[-\frac{625}{48}e_t^3(1+c_i^2)c_{2\beta}\right] + \sin(5\phi-3\phi')\left[-\frac{625}{48}e_t^3(1+c_i^2)s_{2\beta}\right] + \cos(6\phi-4\phi')\left[-\frac{81}{4}e_t^4(1+c_i^2)c_{2\beta}\right] \\
& + \sin(6\phi-4\phi')\left[-\frac{81}{4}e_t^4(1+c_i^2)s_{2\beta}\right] + \cos(\phi-\phi')\left[\left(e_t-\frac{e_t^3}{8}\right)s_i^2\right] + \cos(2\phi-2\phi')\left[\left(e_t^2-\frac{e_t^4}{3}\right)s_i^2\right] \\
& + \cos(3\phi-3\phi')\left[\frac{9}{8}e_t^3 s_i^2\right] + \cos(4\phi-4\phi')\left[\frac{4}{3}e_t^4 s_i^2\right] + \cos(\phi-3\phi')\left[\frac{7}{48}e_t^3(1+c_i^2)c_{2\beta}\right] \\
& + \sin(\phi-3\phi')\left[-\frac{7}{48}e_t^3(1+c_i^2)s_{2\beta}\right] + \cos(2\phi-4\phi')\left[-\frac{1}{8}e_t^4(1+c_i^2)c_{2\beta}\right] + \sin(2\phi-4\phi')\left[-\frac{1}{8}e_t^4(1+c_i^2)s_{2\beta}\right]\Bigg\}, \qquad (2.19)
\end{aligned}
$$

where $\phi = (1+k)l$, $\phi' = kl$, and k provides the rate of the periastron advance per orbit [34]. Further, we let $c_i = \cos\iota$, $s_i = \sin\iota$, $c_{2\beta} = \cos 2\beta$, and $s_{2\beta} = \sin 2\beta$. Note that crucial ingredients to obtain above analytic expressions include developing approaches to solve a PN-accurate Kepler equation and adapting them to derive PN-accurate relations to connect true and eccentric anomalies, detailed in Ref. [45]. A close inspection of the above two equations with Eqs. (3.3) and (3.4) of Ref. [44] reveals that the arguments of cosine and sine functions in the above expressions involve $\phi' = kl$ and its multiples in addition to the usual orbital phase ϕ and its multiples. These additional ϕ' contributions are clearly due to the periastron advance. It turns out that these additional angular contributions are sufficient to provide the numerically inferred side bands in the power spectrum of eccentric binaries due to the presence of k [46]. This is why we explicitly included e_t^4 contributions to the above $h_{\times,+}$ expressions as these contributions are required to reveal the underlying side band structure of waveforms due to the influence of the periastron advance.

We rewrite the above expressions for $h^0_{\times,+}$ in a more compact form to explicitly show how various harmonics are affected by the advance of periastron. The resulting expressions read

$$
\begin{aligned}
h^0_{+,\times}(t) = \Bigg\{ & \sum_{j=1}^{6}[C^{j,-2}_{+,\times}(0)\cos(j\phi-(j-2)\phi') + S^{j,-2}_{+,\times}(0)\sin(j\phi-(j-2)\phi')] + \sum_{j=1}^{4}[C^{j,0}_{+,\times}(0)\cos(j\phi-j\phi') \\
& + S^{j,0}_{+,\times}(0)\sin(j\phi-j\phi')] + \sum_{j=1}^{2}[C^{j,+2}_{+,\times}(0)\cos(j\phi-(j+2)\phi') + S^{j,+2}_{+,\times}(0)\sin(j\phi-(j+2)\phi')]\Bigg\}, \qquad (2.20)
\end{aligned}
$$

where we denoted the coefficient of the $\cos(j\phi-(j\pm n)\phi')$ harmonic at the quadrupolar (Newtonian) order for the $+$ polarization by $C^{j,\pm n}_{+}(0)$ while the coefficient of $\sin(j\phi-(j\pm n)\phi')$ is indicated by $S^{j,\pm n}_{+}(0)$. We adopt a rather heavy notation as it is amenable to higher PN order contributions which will be tackled below. In this convention, we represent the coefficient of $\cos(j\phi-(j\pm n)\phi')$ that appears in the 1PN contributions to $\times$ polarization state by $C^{j,\pm n}_{\times}(1)$. It should be obvious that j stands for the *harmonic* variable while n provides a measure of the shift that each harmonic experiences due to the periastron advance. A close comparison of Eqs. (2.18) and (2.19) reveals that these coefficients are functions of ι, β and contain powers of e_t. Moreover, the arguments of cosine and sine functions clearly show that the eccentricity induced higher *harmonics* are not mere multiples of $\omega = N(1+k)$, where N is the PN-accurate mean motion. Clearly, this is due to the presence of nonvanishing ϕ' contributions due to the periastron advance. Interestingly, the plus polarization state does provide *harmonics* which are integer multiples of N. It is not difficult to show that

these Newtonian-like terms arise from specific cosine functions with arguments $j\phi - j\phi'$, as evident from Eq. (2.19). Further, it is possible to show that these contributions arise from $e_t \cos u s_i^2/(1-e_t\cos u)$ contributions to H^0_+, given by Eq. (F2a) in Ref. [45] and therefore are not influenced by the periastron advance. Interestingly, similar conclusions were obtained in Ref. [46].

With the above inputs, we write the time-domain GW detector response function for eccentric inspirals as

$$h(t) = \frac{Gm\eta}{c^2 D_L} x \Bigg\{ \sum_{j=1}^{6} [\Gamma^{(0)}_{j,-2}\cos(j\phi-(j-2)\phi') + \Sigma^{(0)}_{j,-2}\sin(j\phi-(j-2)\phi')] + \sum_{j=1}^{4}[\Gamma^{(0)}_{j,0}\cos(j\phi-j\phi') + \Sigma^{(0)}_{j,0}\sin(j\phi-j\phi')] + \sum_{j=1}^{2}[\Gamma^{(0)}_{j,+2}\cos(j\phi-(j+2)\phi') + \Sigma^{(0)}_{j,+2}\sin(j\phi-(j+2)\phi')] \Bigg\}, \tag{2.21}$$

where the amplitudes of the cosine and sine functions are denoted by rather complicated symbols $\Gamma^{(0)}_{j,\pm n}$ and $\Sigma^{(0)}_{j,\pm n}$. The definition of $h(t) = F_+ h_+(t) + F_\times h_\times(t)$ ensures that $\Gamma^{(0)}_{j,\pm n} = F_+ C^{j,\pm n}_+(0) + F_\times C^{j,\pm n}_\times(0)$ while $\Sigma^{(0)}_{j,\pm n} = F_+ S^{j,\pm n}_+(0) + F_\times S^{j,\pm n}_\times(0)$. We list in Appendix A the lengthy expressions for these quantities in terms of ι, β and eccentricity contributions, accurate to $\mathcal{O}(e_t^4)$. We display up to $\mathcal{O}(e_t^4)$ contributions to demonstrate the full harmonic structure of the quadrupolar-order GW polarization states. It turns out that $\Sigma^{(0)}_{j,0}$ contributions are zero by construction. This is mainly because the unshifted harmonics only appear with the cosine terms, present in the + polarization state. Invoking familiar trigonometric identities, we simplify the above equation and obtain

$$h(t) = \frac{Gm\eta}{c^2 D_L} x \Bigg\{ \sum_{j=1}^{6} \alpha^{(0)}_{j,-2}\cos(j\phi-(j-2)\phi'+\bar{\phi}^{(0)}_{j,-2}) + \sum_{j=1}^{4} \alpha^{(0)}_{j,0}\cos(j\phi-j\phi'+\bar{\phi}^{(0)}_{j,0}) + \sum_{j=1}^{2} \alpha^{(0)}_{j,+2}\cos(j\phi-(j+2)\phi'+\bar{\phi}^{(0)}_{j,+2}) \Bigg\}, \tag{2.22}$$

where we introduce two new multi-index symbols $\alpha^{(0)}_{j,\pm n}$ and $\bar{\phi}^{(0)}_{j,\pm n}$ to ensure that detector strain can be written in terms of only cosine functions. Influenced by Ref. [44], these symbols are defined as $\alpha^{(0)}_{j,\pm n} = \text{sign}(\Gamma^{(0)}_{j,\pm n})\sqrt{(\Gamma^{(0)}_{j,\pm n})^2 + (\Sigma^{(0)}_{j,\pm n})^2}$ and $\bar{\phi}^{(0)}_{j,\pm n} = \tan^{-1}(-\frac{\Sigma^{(0)}_{j,\pm n}}{\Gamma^{(0)}_{j,\pm n}})$. We do not list explicit expressions for these quantities that are accurate to $\mathcal{O}(e_t^4)$ in eccentricity corrections as they can be easily obtained from our Eqs. (A1) and (A2).

A close inspection of the above equations reveals that they provide the GW response function for compact binaries moving along precessing eccentric orbits. To obtain temporally evolving $h(t)$ associated with compact binaries inspiraling along precessing eccentric orbits, we need to specify how ϕ, ϕ', ω and e_t vary in time due to GW emission. We adapt the phasing formalism, detailed in Refs. [34,49], to provide differential equations for these variables. And, for the time being, we will concentrate on the secular evolution of these variables. In other words, we will neglect GW induced quasiperiodic variations to orbital elements and angles, detailed in Ref. [34]. The 3PN-accurate secular evolution to ϕ and ϕ' in the modified harmonic gauge that are accurate to $\mathcal{O}(e_t^6)$ is given by

$$\frac{d\phi}{dt} = \omega = x^{3/2}\frac{c^3}{Gm}, \tag{2.23}$$

$$\frac{d\phi'}{dt} = \omega\frac{k}{1+k} = \omega\Bigg\{3x[1+e_t^2+e_t^4+e_t^6] + x^2\left[\frac{9}{2}-7\eta+\left(\frac{87}{4}-\frac{41}{2}\eta\right)e_t^2+(39-34\eta)e_t^4+\left(\frac{225}{4}-\frac{95}{2}\eta\right)e_t^6\right] + x^3\left[\frac{27}{2}+\left(-\frac{481}{4}+\frac{123\pi^2}{32}\right)\eta+7\eta^2+\left(\frac{519}{4}+\left(-\frac{2037}{4}+\frac{1599\pi^2}{128}\right)\eta+61\eta^2\right)e_t^2+\left(\frac{2811}{8}+\left(-1174+\frac{3321\pi^2}{128}\right)\eta+\frac{1361}{8}\eta^2\right)e_t^4+\left(\frac{10779}{16}+\left(-\frac{16901}{8}+\frac{2829\pi^2}{64}\right)\eta+\frac{2675}{8}\eta^2\right)e_t^6\right]\Bigg\}, \tag{2.24}$$

$$\frac{d\omega}{dt} = \frac{96c^6\eta}{5G^2m^2}x^{11/2}\Bigg\{1+\frac{157}{24}e_t^2+\frac{605}{32}e_t^4+\frac{3815}{96}e_t^6+x\left[-\frac{743}{336}-\frac{11}{4}\eta+\left(\frac{713}{112}-\frac{673}{16}\eta\right)e_t^2+\left(\frac{52333}{672}-\frac{12415}{64}\eta\right)e_t^4+\left(\frac{13823}{48}-\frac{107765}{192}\eta\right)e_t^6\right]+\dot{\omega}^{1.5PN}+\dot{\omega}^{2PN}+\dot{\omega}^{2.5PN}+\dot{\omega}^{3PN}\Bigg\}, \tag{2.25}$$

$$\frac{de_t}{dt} = -\frac{304c^3\eta e_t}{15Gm}x^4\left\{1+\frac{881}{304}e_t^2+\frac{3265}{608}e_t^4+\frac{20195}{2432}e_t^6+x\left[-\frac{2817}{2128}-\frac{1021}{228}\eta+\left(\frac{40115}{4256}-\frac{51847}{1824}\eta\right)e_t^2\right.\right.$$
$$\left.\left.+\left(\frac{87749}{2128}-\frac{298115}{3648}\eta\right)e_t^4+\left(\frac{121833}{1216}-\frac{2501905}{14592}\eta\right)e_t^6\right]+\dot{e}_t^{1.5PN}+\dot{e}_t^{2PN}+\dot{e}_t^{2.5PN}+\dot{e}_t^{3PN}\right\}. \quad (2.26)$$

The explicit 1.5,2,2.5, and 3PN order contributions to $d\omega/dt$ and de_t/dt that incorporate all the $\mathcal{O}(e_t^6)$ corrections are provided in the Appendix B. The differential equations for $d\omega/dt$ and de_t/dt are extracted from expressions, available in Refs. [50,51] and are in the modified harmonic gauge. These papers provided above 3PN-accurate expressions as the sum of certain "instantaneous" and "tail" contributions

$$\frac{d\omega}{dt} = \left(\frac{d\omega}{dt}\right)_{\text{inst}} + \left(\frac{d\omega}{dt}\right)_{\text{tail}},$$
$$\frac{de_t}{dt} = \left(\frac{de_t}{dt}\right)_{\text{inst}} + \left(\frac{de_t}{dt}\right)_{\text{tail}}.$$

The 3PN-accurate instantaneous contributions depend only on the binary dynamics at the usual retarded time while the hereditary contributions are sensitive to the binary dynamics at all epochs prior to the usual retarded time [64]. The instantaneous contributions to $d\omega/dt$ are extracted from Eqs. (6.14), (6.15a), (6.15), (C6), and (C7) of Ref. [50] while for de_t/dt such contributions originate from Eqs. (6.16), (6.19a), (6.19b), (C10), and (C11) in Ref. [50]. It should be obvious that we have Taylor expanded these equations around $e_t = 0$ to obtain eccentricity contributions accurate to $\mathcal{O}(e_t^6)$. The hereditary contributions to $d\omega/dt$ and de_t/dt are adapted from Eqs. (6.24c) and (6.26) of Ref. [50] and they depend on a number of eccentricity enhancement functions. We employ such enhancement functions provided in Ref. [51] for our computations. We now have all the inputs to obtain the restricted time-domain $h(t)$ to model GWs from nonspinning compact binaries inspiraling along precessing moderately eccentric orbits. To obtain such time-domain templates, we numerically solve the above listed differential equations for ω, e_t, ϕ, and ϕ' and impose their temporal evolution in the quadrupolar-order GW response function, given by Eq. (2.22). We now move on to describe how we extend the quadrupolar-order GW response function.

It should be obvious that we require a prescription to compute analytically PN-accurate amplitude-corrected GW polarization states to improve the above listed quadrupolar-order GW response function. Therefore, we adapt 1PN-accurate amplitude-corrected and fully analytic expressions for $h_{\times,+}$, available in Ref. [45], to compute GW response function for eccentric inspirals that incorporates PN contributions even to its amplitudes. We list below certain ingredients that will be crucial to write down analytic $h(t)$ that incorporates 1PN-accurate amplitude corrections to $h_{\times,+}$ while consistently keeping eccentricity contributions up to $\mathcal{O}(e_t^6)$. We begin by displaying Eqs. (44) and (45) of Ref. [45] as a single sum which reads

$$h_{+,\times}(t) = \frac{Gm\eta}{c^2 D_L}x\{h^0_{+,\times}(t) + x^{0.5}h^{0.5}_{+,\times}(t) + xh^1_{+,\times}(t)\}. \quad (2.27)$$

Various PN order amplitude contributions take the following form:

$$h^0_{+,\times}(t) = \sum_{j=1}^{8}\{C^{j,-2}_{+,\times}(0)\cos(j\phi-(j-2)\phi') + S^{j,-2}_{+,\times}(0)\sin(j\phi-(j-2)\phi')\} + \sum_{j=1}^{6}\{C^{j,0}_{+,\times}(0)\cos(j\phi-j\phi')$$
$$+ S^{j,0}_{+,\times}(0)\sin(j\phi-j\phi')\} + \sum_{j=1}^{4}\{C^{j,+2}_{+,\times}(0)\cos(j\phi-(j+2)\phi') + S^{j,+2}_{+,\times}(0)\sin(j\phi-(j+2)\phi')\}, \quad (2.28a)$$

$$h^{0.5}_{+,\times}(t) = \delta\left\{\sum_{j=1}^{7}[C^{j,-1}_{+,\times}(0.5)\cos(j\phi-(j-1)\phi') + S^{j,-1}_{+,\times}(0.5)\sin(j\phi-(j-1)\phi')] + \sum_{j=1}^{5}[C^{j,+1}_{+,\times}(0.5)\cos(j\phi-(j+1)\phi')\right.$$
$$+ S^{j,+1}_{+,\times}(0.5)\sin(j\phi-(j+1)\phi')] + \sum_{j=1}^{9}[C^{j,-3}_{+,\times}(0.5)\cos(j\phi-(j-3)\phi') + S^{j,-3}_{+,\times}(0.5)\sin(j\phi-(j-3)\phi')]$$
$$\left.+\sum_{j=1}^{3}[C^{j,+3}_{+,\times}(0.5)\cos(j\phi-(j+3)\phi') + S^{j,+3}_{+,\times}(0.5)\sin(j\phi-(j+3)\phi')]\right\}, \quad (2.28b)$$

$$h^{1}_{+,\times}(t) = \sum_{j=1}^{8}\{C^{j,-2}_{+,\times}(1)\cos(j\phi-(j-2)\phi') + S^{j,-2}_{+,\times}(1)\sin(j\phi-(j-2)\phi')\} + \sum_{j=1}^{4}\{C^{j,+2}_{+,\times}(1)\cos(j\phi-(j+2)\phi')$$
$$+ S^{j,+2}_{+,\times}(1)\sin(j\phi-(j+2)\phi')\} + \sum_{j=1}^{10}\{C^{j,-4}_{+,\times}(1)\cos(j\phi-(j-4)\phi') + S^{j,-4}_{+,\times}(1)\sin(j\phi-(j-4)\phi')\}$$
$$+ \sum_{j=1}^{2}\{C^{j,+4}_{+,\times}(1)\cos(j\phi-(j+4)\phi') + S^{j,+4}_{+,\times}(1)\sin(j\phi-(j+4)\phi')\} + \sum_{j=1}^{6}\{C^{j,0}_{+,\times}(1)\cos(j\phi-j\phi')$$
$$+ S^{j,0}_{+,\times}(1)\sin(j\phi-j\phi')\}, \tag{2.28c}$$

where $\delta = (m_1 - m_2)/(m_1 + m_2)$ and we let m_1 be the heavier of the two binary components. We do not list explicitly very lengthy expressions for these amplitudes. However, they can be easily extracted from the attached Mathematica notebook [65]. The derivation of the above lengthy expressions includes developing analytic approaches to solve the PN-accurate Kepler equation and PN-accurate relations connecting true and eccentric anomalies, detailed in Ref. [45]. Indeed, we have verified that these expressions reduce to their circular counterparts, provided in Ref. [66].

The associated GW detector strain for eccentric binaries is given by

$$h(t) = \frac{Gm\eta}{c^2 D_L} x\Bigg\{\Bigg[\sum_{j=1}^{8}(\Gamma^{(0)}_{j,-2}\cos(j\phi-(j-2)\phi') + \Sigma^{(0)}_{j,-2}\sin(j\phi-(j-2)\phi')) + \sum_{j=1}^{6}(\Gamma^{(0)}_{j,0}\cos(j\phi-j\phi') + \Sigma^{(0)}_{j,0}\sin(j\phi-j\phi'))$$
$$+ \sum_{j=1}^{4}(\Gamma^{(0)}_{j,+2}\cos(j\phi-(j+2)\phi') + \Sigma^{(0)}_{j,+2}\sin(j\phi-(j+2)\phi'))\Bigg] + x^{0.5}\delta\Bigg[\sum_{j=1}^{7}(\Gamma^{(0.5)}_{j,-1}\cos(j\phi-(j-1)\phi')$$
$$+ \Sigma^{(0.5)}_{j,-1}\sin(j\phi-(j-1)\phi')) + \sum_{j=1}^{5}(\Gamma^{(0.5)}_{j,+1}\cos(j\phi-(j+1)\phi') + \Sigma^{(0.5)}_{j,+1}\sin(j\phi-(j+1)\phi'))$$
$$+ \sum_{j=1}^{9}(\Gamma^{(0.5)}_{j,-3}\cos(j\phi-(j-3)\phi') + \Sigma^{(0.5)}_{j,-3}\sin(j\phi-(j-3)\phi')) + \sum_{j=1}^{3}(\Gamma^{(0.5)}_{j,+3}\cos(j\phi-(j+3)\phi')$$
$$+ \Sigma^{(0.5)}_{j,+3}\sin(j\phi-(j+3)\phi'))\Bigg] + x\Bigg[\sum_{j=1}^{8}(\Gamma^{(1)}_{j,-2}\cos(j\phi-(j-2)\phi') + \Sigma^{(1)}_{j,-2}\sin(j\phi-(j-2)\phi'))$$
$$+ \sum_{j=1}^{4}(\Gamma^{(1)}_{j,+2}\cos(j\phi-(j+2)\phi') + \Sigma^{(1)}_{j,+2}\sin(j\phi-(j+2)\phi')) + \sum_{j=1}^{6}(\Gamma^{(1)}_{j,0}\cos(j\phi-j\phi') + \Sigma^{(1)}_{j,0}\sin(j\phi-j\phi'))$$
$$+ \sum_{j=1}^{10}(\Gamma^{(1)}_{j,-4}\cos(j\phi-(j-4)\phi') + \Sigma^{(1)}_{j,-4}\sin(j\phi-(j-4)\phi')) + \sum_{j=1}^{2}(\Gamma^{(1)}_{j,+4}\cos(j\phi-(j+4)\phi')$$
$$+ \Sigma^{(1)}_{j,+4}\sin(j\phi-(j+4)\phi'))\Bigg]\Bigg\}, \tag{2.29}$$

where, as expected, we have defined

$$\Gamma^{(p)}_{j,\pm n} = F_+ C^{j,\pm n}_+(p) + F_\times C^{j,\pm n}_\times(p), \tag{2.30a}$$

$$\Sigma^{(p)}_{j,\pm n} = F_+ S^{j,\pm n}_+(p) + F_\times S^{j,\pm n}_\times(p). \tag{2.30b}$$

A further simplification is possible which requires, as expected, additional multi-index functions such that

$$\alpha^{(p)}_{j,\pm n} = \mathrm{sign}(\Gamma^{(p)}_{j,\pm n})\sqrt{(\Gamma^{(p)}_{j,\pm n})^2 + (\Sigma^{(p)}_{j,\pm n})^2}, \tag{2.31a}$$

$$\bar{\phi}^{(p)}_{j,\pm n} = \tan^{-1}\left(-\frac{\Sigma^{(p)}_{j,\pm n}}{\Gamma^{(p)}_{j,\pm n}}\right), \tag{2.31b}$$

$$h(t) = \frac{Gm\eta}{c^2 D_L} x \Bigg\{ \Bigg[\sum_{j=1}^{8} \alpha_{j,-2}^{(0)} \cos(j\phi - (j-2)\phi' + \bar{\phi}_{j,-2}^{(0)}) + \sum_{j=1}^{6} \alpha_{j,0}^{(0)} \cos(j\phi - j\phi' + \bar{\phi}_{j,0}^{(0)}) + \sum_{j=1}^{4} \alpha_{j,+2}^{(0)} \cos(j\phi - (j+2)\phi' + \bar{\phi}_{j,+2}^{(0)}) \Bigg] + x^{0.5}\delta \Bigg[\sum_{j=1}^{7} \alpha_{j,-1}^{(0.5)} \cos(j\phi - (j-1)\phi' + \bar{\phi}_{j,-1}^{(0.5)}) + \sum_{j=1}^{5} \alpha_{j,+1}^{(0.5)} \cos(j\phi - (j+1)\phi' + \bar{\phi}_{j,-1}^{(0.5)}) + \sum_{j=1}^{9} \alpha_{j,-3}^{(0.5)} \cos(j\phi - (j-3)\phi' + \bar{\phi}_{j,-3}^{(0.5)}) + \sum_{j=1}^{3} \alpha_{j,+3}^{(0.5)} \cos(j\phi - (j+3)\phi' + \bar{\phi}_{j,+3}^{(0.5)}) \Bigg] + x \Bigg[\sum_{j=1}^{8} \alpha_{j,-2}^{(1)} \cos(j\phi - (j-2)\phi' + \bar{\phi}_{j,-2}^{(1)}) + \sum_{j=1}^{4} \alpha_{j,+2}^{(1)} \cos(j\phi - (j+2)\phi' + \bar{\phi}_{j,+2}^{(1)}) + \sum_{j=1}^{6} \alpha_{j,0}^{(1)} \cos(j\phi - j\phi' + \bar{\phi}_{j,0}^{(1)}) + \sum_{j=1}^{10} \alpha_{j,-4}^{(1)} \cos(j\phi - (j-4)\phi' + \bar{\phi}_{j,-4}^{(1)}) + \sum_{j=1}^{2} \alpha_{j,+4}^{(1)} \cos(j\phi - (j+4)\phi' + \bar{\phi}_{j,+4}^{(1)}) \Bigg] \Bigg\}. \tag{2.32}$$

A cursory look at the above equation may give the impression that the summation indices in various sums are terminated in an arbitrary manner. Interestingly, we find a possible way to predict the maximum value that j index can take in each of the above summations. This is related to the argument of ϕ' in each of these cosine series. We infer that the argument of ϕ' can take a maximum value of six as we are restricting eccentricity contributions to sixth order in e_t. This ensures that the j index can take maximum values of 8,6, and 4 at the Newtonian order in the above expression. In other words, $j_{\rm max}$ in the above expression is given such that $j_{\rm max} \pm n = 6$ where the $\pm n$ value arises from the argument of the ϕ' variable in various summations. It is easy to see that the above relation holds true even at 0.5 and 1PN orders and it provides a natural check on the structure of these higher-order PN contributions to $h(t)$.

To obtain the GW response function for eccentric inspirals, we need to incorporate the temporal evolution in ω, e_t, ϕ, and ϕ', given by our earlier listed 3PN-accurate differential equations. The fact that we are required to solve the above four coupled differential equations numerically ensures that our approach to obtain ready-to-use $h(t)$ will be computationally expensive. This is clearly one of the motivations to obtain fully analytic $\tilde{h}(f)$ for compact binaries inspiraling along moderately eccentric orbits. Fortunately, we are in a position to compute analytic amplitude-corrected $\tilde{h}(f)$ that incorporates the 3PN-accurate Fourier phase while keeping eccentricity contributions accurate to sixth order in e_0 at every PN order.

III. ANALYTIC $\tilde{h}(f)$ FOR ECCENTRIC INSPIRALS WITH 1PN AMPLITUDE CORRECTIONS

We first provide a detailed description of our approach to compute the analytic Fourier transform of the restricted time-domain inspiral family, given by Eq. (2.22). This will be followed by computing $\tilde{h}(f)$ associated with Eq. (2.32). Preliminary data analysis implications of our analytic $\tilde{h}(f)$ are probed in Sec. III B.

A. Approach to compute Fourier transform of $h(t)$ for compact binaries inspiraling along precessing eccentric orbits

We begin by listing the expanded version of our quadrupolar-order $h(t)$, namely, Eq. (2.22) with $\mathcal{O}(e_t^4)$ eccentricity contributions as

$$h(t) = \frac{Gm\eta}{c^2 D_L} x \{ [\alpha_{1,-2}^{(0)} \cos(\phi + \phi' + \bar{\phi}_{1,-2}^{(0)}) + \alpha_{2,-2}^{(0)} \cos(2\phi + \bar{\phi}_{2,-2}^{(0)}) + \alpha_{3,-2}^{(0)} \cos(3\phi - \phi' + \bar{\phi}_{3,-2}^{(0)}) + \alpha_{4,-2}^{(0)} \cos(4\phi - 2\phi' + \bar{\phi}_{4,-2}^{(0)}) + \alpha_{5,-2}^{(0)} \cos(5\phi - 3\phi' + \bar{\phi}_{5,-2}^{(0)}) + \alpha_{6,-2}^{(0)} \cos(6\phi - 4\phi' + \bar{\phi}_{6,-2}^{(0)})] + [\alpha_{1,0}^{(0)} \cos(\phi - \phi' + \bar{\phi}_{1,0}^{(0)}) + \alpha_{2,0}^{(0)} \cos(2\phi - 2\phi' + \bar{\phi}_{2,0}^{(0)}) + \alpha_{3,0}^{(0)} \cos(3\phi - 3\phi' + \bar{\phi}_{3,0}^{(0)}) + \alpha_{4,0}^{(0)} \cos(4\phi - 4\phi' + \bar{\phi}_{4,0}^{(0)})] + [\alpha_{1,+2}^{(0)} \cos(\phi - 3\phi' + \bar{\phi}_{1,+2}^{(0)}) + \alpha_{2,+2}^{(0)} \cos(2\phi - 4\phi' + \bar{\phi}_{2,+2}^{(0)})] \}. \tag{3.1}$$

Clearly, we see three distinct square brackets that contain three cosine functions with explicitly time dependent arguments, namely, $j\phi-(j-2)\phi'$, $j\phi-j\phi'$, and $j\phi-(j+2)\phi'$. Note that $\alpha^{(0)}_{j,\pm n}$ and $\bar{\phi}^{(0)}_{j,\pm n}$ experience implicit temporal evolution due to the GW emission induced variations to ω and e_t. The main reason for displaying the above equation is to show explicitly how the periastron advance, defined by ϕ', influences the harmonic structure of $h(t)$ in comparison with Eq. (4.21) of Ref. [44] or our Eq. (2.3).

We obtain an analytic Fourier domain version of the above equation with the help of the stationary phase approximation, detailed in [62]. How this approach can be employed to compute $\tilde{h}(f)$ for compact binaries spiraling along Keplerian eccentric orbits can be found in Sec. IV of Ref. [44]. This approximation is quite appropriate for us as it provides a prescription to compute the asymptotic behavior of the generalized cosine time series, as given by our Eq. (3.1). Without loss of any generality, we may write such a time series as

$$S(t)=s(t)\cos(l\phi(t)), \tag{3.2}$$

where $l>0$ and as expected $S(t)$ should be a product of slowly varying amplitude $s(t)$ and a rapidly varying cosine function with argument $l\phi(t)$. Because of the virtue of the Riemann-Lebesgue lemma, as noted in Ref. [62], the Fourier transform of $S(t)$ becomes

$$S_f(f)=\frac{1}{2}\int_{-\infty}^{\infty}s(t)e^{if(2\pi t-l\phi(t)/f)}dt. \tag{3.3}$$

It is not difficult to gather that the argument of the exponential function vanishes at the stationary point t_0 such that $l\dot{\phi}(t_0)=2\pi f$. This allows us to invoke the approach of SPA to obtain the asymptotic behavior of $S_f(f)$ by the following expression:

$$\begin{aligned}S_f(f)&=s(t_0)e^{-i\Psi(t_0)\pm i\pi/(2\times 2)}\left[\frac{2!}{f|\Psi^{(2)}(t_0)|}\right]^{\frac{1}{2}}\frac{\Gamma(1/2)}{2}\\&=\frac{s(t_0)}{2\sqrt{l\dot{F}(t_0)}}e^{-i(\Psi(t_0)\mp\pi/4)},\end{aligned} \tag{3.4}$$

where the Fourier phase is defined as

$$\Psi(t):=-2\pi ft+l\phi(t).$$

Note that $F(t)=\dot{\phi}(t)/2\pi$ and therefore its value at the stationary point should be $F(t_0)=f/l$. Interestingly, a rather identical computation can be done to obtain the Fourier transform of a similar sinusoidal time series to be $iS_f(f)$.

To make operational the above expression for $S_f(f)$, we require an explicit expression for the above defined Fourier phase at the stationary point t_0, namely,

$$\Psi(t_0):=-2\pi ft_0+l\phi(t_0). \tag{3.5}$$

This is done by defining $\tau=F/\dot{F}$ such that $\phi(F)$ and $t(F)$ become

$$\phi(F)=\phi_c+2\pi\int^F\tau' dF', \tag{3.6}$$

$$t(F)=t_c+\int^F\frac{\tau'}{F'}dF', \tag{3.7}$$

where ϕ_c and t_c are the orbital phase and time at coalescence. In the present context, τ is defined using our 3PN-accurate expression for $\dot{\omega}$ given by Eq. (2.25). Additionally, we require the 3PN-accurate $e_t(\omega,\omega_0,e_0)$ expression, namely, the 3PN extension of Eq. (2.16), for computing these integrals analytically. The expression for $\Psi[F(t_0)]$ obtained using Eqs. (3.6) and (3.7) in (3.5) may be written as

$$\Psi_l[F(t_0)]=l\phi_c-2\pi ft_c+2\pi\int^{F(t_0)}\tau'\left(l-\frac{f}{F'}\right)dF', \tag{3.8}$$

where $F(t_0)=f/l$. In the present context, we need to evaluate the above integral at a point of time where the orbital frequency is related to the Fourier frequency by $F(t_0)=f/l$. A close inspection of Eq. (3.1) reveals that our expression for the quadrupolar-order time-domain response function is structurally similar to the above displayed cosine time series and therefore we can easily adapt these results to obtain the Fourier transform of our quadrupolar-order $h(t)$. However, the SPA based $\tilde{h}(f)$ will have contributions from a number of distinct stationary points. This is primarily due to the fact that Eq. (3.1) consists of cosine functions of three different arguments, namely, $j\phi-(j+2)\phi'$, $j\phi-(j-2)\phi'$ and $j\phi-j\phi'$. Note that there are only three distinct types of cosine arguments as we restricted our attention to the quadrupolar-order GW response function for eccentric inspirals. However, we infer from our 1PN-accurate $h(t)$, given by Eq. (2.32), that there are *nine* distinct types of cosine functions with arguments $j\phi-(j\pm n)\phi'$ where $n=0,1,2,3,4$. The associated *nine* stationary points $t^{\pm n}$ are computed by demanding that $\dot{\Psi}^{\pm n}(t^{\pm n})=0$, where $\Psi^{\pm n}(t):=-2\pi ft+j\phi-(j\pm n)\phi'$.

For computing the Fourier transform of Eq. (3.1), we solve $\dot{\Psi}^{\pm n}(t^{\pm n})=0$ to get the relevant stationary points and this leads to

$$-2\pi f+j\dot{\phi}-(j\pm n)\dot{\phi}'=0, \tag{3.9}$$

where $\dot{\phi} = N(1+k)$ and this by definition is ω. The treatment of $\dot{\phi}'$ requires the PN approximation as $\dot{\phi}'$ equals kN (this is because $\phi' = kl$). We need to express kN in terms of ω and this leads to $\dot{\phi}' = \omega k/(1+k)$ as $\omega = N(1+k)$. For computing the Fourier phase analytically, we express $\dot{\phi}'$ as $\omega k^{(6)}_{(3)}$, where $k^{(6)}_{(3)}$ stands for the 3PN-accurate expression for $k/(1+k)$ that incorporates e_t contributions accurate to $\mathcal{O}(e_t^6)$. The resulting expression reads

$$k^{(6)}_{(3)} = x\{3[1+e_t^2+e_t^4+e_t^6]\} + x^2\left\{\frac{9}{2} - 7\eta + \left[\frac{87}{4} - \frac{41\eta}{2}\right]e_t^2 + [39-34\eta]e_t^4 + \left[\frac{225}{4} - \frac{95\eta}{2}\right]e_t^6\right\} + x^3\left\{\frac{27}{2}\right.$$
$$+ \left(-\frac{481}{4} + \frac{123\pi^2}{32}\right)\eta + 7\eta^2 + \left[\frac{519}{4} + \left(-\frac{2037}{4} + \frac{1599\pi^2}{128}\right)\eta + 61\eta^2\right]e_t^2 + \left[\frac{2811}{8} + \left(-1174 + \frac{3321\pi^2}{128}\right)\eta\right.$$
$$\left.\left. + \frac{1361}{8}\eta^2\right]e_t^4 + \left[\frac{10779}{16} + \left(-\frac{16901}{8} + \frac{2829\pi^2}{64}\right)\eta + \frac{2675}{8}\eta^2\right]e_t^6\right\}. \tag{3.10}$$

With the help of these inputs, the stationary points $t^{\pm n}$, where $\dot{\Psi}^{\pm n}(t^{\pm n})$ vanish, are given by

$$(j - (j \pm n)k^{(6)}_{(3)})\dot{\phi}(t^{\pm n}) = 2\pi f.$$

In other words, the stationary phase condition is given by

$$F(t^{\pm n}) = \frac{f}{(j - (j \pm n)k^{(6)}_{(3)})}. \tag{3.11}$$

Rewriting $\Psi^{\pm n}(t) \coloneqq -2\pi f t + j\phi - (j \pm n)\phi'$ using the relation between ϕ' and ϕ ($\phi' = k^{(6)}_{(3)}\phi$) gives $\Psi^{\pm n}(t) \coloneqq -2\pi f t + (j - (j \pm n)k^{(6)}_{(3)})\phi$. We are now in a position to obtain analytic PN-accurate expressions for the Fourier phases associated with these stationary points. With Eqs. (3.6) and (3.7), our Eq. (3.8) becomes

$$\Psi^{\pm n}_j[F(t^{\pm n})] = (j - (j \pm n)k^{(6)}_{(3)})\phi_c - 2\pi f t_c + 2\pi \int^{F(t^{\pm n})} \tau'\left(j - (j \pm n)k^{(6)}_{(3)} - \frac{f}{F'}\right)dF'. \tag{3.12}$$

Note that n takes values 0 and 2 as we are dealing with the quadrupolar-order GW response function given by Eq. (3.1). However, n varies from 0 to 4 if the underlying GW response function contains 1PN-accurate amplitude corrections that include at each PN order eccentricity corrections accurate to $\mathcal{O}(e_t^6)$. Further, we do not display here the 3PN-accurate expression for τ that includes the leading-order e_t corrections, listed as Eqs. (6.7a) and (6.7b) in Ref. [63]. However, we do list below the explicit 3PN-accurate $\Psi^{\pm n}_j[F(t^{\pm n})]$ that incorporates leading-order e_0 contributions at each PN order:

$$\Psi^n_j = (j - (j+n)k^{(6)}_{(3)})\phi_c - 2\pi f t_c - \frac{3j}{256\eta x^{5/2}}\left\{1 - \frac{2355}{1462}e_0^2\chi^{-19/9} + x\left[-\frac{2585}{756} - \frac{25n}{3j} + \frac{55}{9}\eta\right.\right.$$
$$+ \left(\left(\frac{69114725}{14968128} + \frac{1805n}{172j} - \frac{128365}{12432}\eta\right)\chi^{-19/9} + \left(-\frac{2223905}{491232} + \frac{15464}{17544}\eta\right)\chi^{-25/9}\right)e_0^2\Big]\Big\} + x^{3/2}\Big[-16\pi$$
$$+ \left(\frac{65561\pi}{4080}\chi^{-19/9} - \frac{295945\pi}{35088}\chi^{-28/9}\right)e_0^2\Big] + x^2\left[-\frac{48825515}{508032} - \frac{31805n}{252j} + \left(\frac{22105}{504} - \frac{10n}{j}\right)\eta + \frac{3085}{72}\eta^2\right.$$
$$+ \left(\left(\frac{115250777195}{2045440512} + \frac{323580365n}{5040288j} + \left(-\frac{72324815665}{6562454976} + \frac{36539875n}{1260072j}\right)\eta - \frac{10688155}{294624}\eta^2\right)\chi^{-19/9}\right.$$
$$+ \left(\frac{195802015925}{15087873024} + \frac{5113565n}{173376j} + \left(-\frac{3656612095}{67356576} - \frac{355585n}{6192j}\right)\eta + \frac{25287905}{447552}\eta^2\right)\chi^{-25/9} + \left(\frac{936702035}{1485485568}\right.$$
$$\left.\left.\left. + \frac{3062285}{260064}\eta - \frac{14251675}{631584}\eta^2\right)\chi^{-31/9}\right)e_0^2\Big] + x^{5/2}\left[\frac{14453\pi}{756} - \frac{32\pi n}{j} - \frac{65\pi}{9}\eta - \left(\frac{1675}{756} + \frac{160n}{3j} + \frac{65}{9}\eta\right)\pi\log\left(\frac{f}{j}\right)\right.$$
$$+ \left(\left(-\frac{458370775\pi}{6837264} - \frac{4909969\pi n}{46512j} + \frac{15803101\pi\eta}{229824}\right)\chi^{-19/9} + \left(\frac{185734313\pi}{4112640} - \frac{12915517\pi\eta}{146880}\right)\chi^{-25/9}\right.$$

$$+\left(\frac{26056251325\pi}{1077705216}+\frac{680485\pi n}{12384j}-\frac{48393605\pi\eta}{895104}\right)\chi^{-28/9}+\left(-\frac{7063901\pi}{520128}+\frac{149064749\pi\eta}{2210544}\right)\chi^{-34/9}\Bigg)e_0^2\Bigg]$$
$$+x^3\Bigg[\frac{13966988843531}{4694215680}+\frac{257982425n}{508032j}-\frac{640\pi^2}{3}-\frac{6848\gamma}{21}+\left(-\frac{20562265315}{3048192}-\frac{2393105n}{1512j}+\frac{23575\pi^2}{96}$$
$$+\frac{1845\pi^2 n}{32j}\right)\eta+\left(\frac{110255}{1728}+\frac{475n}{24j}\right)\eta^2-\frac{127825\eta^3}{1296}-\frac{13696\log(2)}{21}-\frac{3424\log(x)}{21}$$
$$+\Bigg(\left(\frac{4175723876720788380517}{5556561877278720000}+\frac{534109712725265n}{2405438042112j}-\frac{21508213\pi^2}{276480}-\frac{734341\gamma}{16800}+\left(-\frac{37399145056383727}{28865256505344}\right.\right.$$
$$\left.-\frac{1219797059185n}{2045440512j}+\frac{12111605\pi^2}{264192}+\frac{639805n\pi^2}{22016j}\right)\eta+\left(-\frac{159596464273381}{1718170030080}+\frac{43766986495n}{1022720256j}\right)\eta^2-\frac{69237581}{746496}\eta^3$$
$$\left.-\frac{9663919\log(2)}{50400}+\frac{4602177\log(3)}{44800}-\frac{734341\log(x)}{33600}\right)\chi^{-19/9}+\left(\frac{326505451793435}{2061804036096}+\frac{916703174045n}{5080610304j}\right.$$
$$\left.-\left(\frac{13467050491570355}{39689727694848}+\frac{9519440485n}{35282016j}\right)\eta-\left(\frac{2186530635995}{52499639808}+\frac{7198355375n}{45362592j}\right)\eta^2+\frac{2105566535}{10606464}\eta^3\right)\chi^{-25/9}$$
$$+\frac{24716497\pi^2}{293760}\chi^{-28/9}+\left(-\frac{82471214720975}{45625728024576}-\frac{2153818055n}{524289024j}+\left(-\frac{48415393035455}{1629490286592}-\frac{119702185n}{1560384j}\right)\eta\right.$$
$$\left.+\left(\frac{906325428545}{6466231296}+\frac{32769775n}{222912j}\right)\eta^2-\frac{2330466575}{16111872}\eta^3\right)\chi^{-31/9}+\left(-\frac{4165508390854487}{16471063977984}-\frac{96423905\pi^2}{5052672}\right.$$
$$+\frac{2603845\gamma}{61404}+\left(-\frac{1437364085977}{53477480448}+\frac{3121945\pi^2}{561408}\right)\eta+\frac{4499991305\eta^2}{636636672}+\frac{2425890995\eta^3}{68211072}+\frac{1898287\log(2)}{184212}$$
$$\left.+\frac{12246471\log(3)}{163744}+\frac{2603845\log(x)}{122808}-\frac{2603845\log(\chi)}{184212}\right)\chi^{-37/9}\Bigg)e_0^2\Bigg]. \tag{3.13}$$

A few comments are in order. To obtain the circular limit, we require imposing $n=j$ in $j\phi-(j-n)\phi'$ and then letting $e_0=0$. This is indeed due to the fact that $k^{(6)}_{(3)}$ does not go to zero in the circular limit. Additionally, we have verified that the resulting $\Psi^{-2}_2(f)$ expression in the $e_0\to 0$ limit is identical to the 3PN-accurate version of Eq. (6.26) in Ref. [63] while neglecting the spin contributions. It is natural to expect that the $\Psi^0_j(f)$ version of our above equation should be identical to Eq. (6.26) of Ref. [63]. This is because this equation indeed provided quadrupolar $\tilde{h}(f)$ with the 3PN-accurate Fourier phase while incorporating leading-order e_0 corrections at each PN order by extending the postcircular approach of Ref. [44]. However, our expression for $\Psi^0_j(f)$ is not identical to Eq. (6.26) of Ref. [63]. This is because that effort did not incorporate the effect of the periastron advance while obtaining the analytic expression for their Fourier phase. A close inspection of the $n=0$ version of our Eq. (3.12) reveals that it will still be influenced by our PN-accurate expression for $k^{(6)}_{(3)}$. This clearly shows that it is rather impossible to remove the effect of the periastron advance from our Eq. (3.12). Therefore, our Eq. (3.13) will be different from Eq. (6.26) of Ref. [63] which, as noted earlier, neglected the effect of the periastron advance. The differences may be attributed to the physical fact that we are providing an analytic expression for $\tilde{h}(f)$ associated with compact binaries inspiraling along PN-accurate eccentric orbits. In contrast, Ref. [63] models inspiral GWs from compact binaries spiraling in along Newtonian orbits though frequency evolution in both cases are fully 3PN accurate. Additionally, we are unable to match with the 2PN order results of Ref. [49] due to similar reasons. We note in passing that the explicit 3PN-accurate $\mathcal{O}(e_0^4)$ contributions to $\Psi^n_j(f)$ and the associated 3PN-accurate e_t expression are provided in Appendix C.

We now employ fully the final result of SPA, namely, Eq. (3.4), to compute the Fourier transform of Eq. (3.1). This gives us

$$\tilde{h}[F(t_0)] = \left(\frac{5\pi\eta}{384}\right)^{1/2} \frac{G^2m^2}{c^5 D_L} \left(\frac{Gm\pi 2F(t_0)}{c^3}\right)^{-7/6} \frac{(1-e_t^2)^{7/4}}{(1+\frac{73}{24}e_t^2+\frac{37}{96}e_t^4)^{1/2}} \left\{ \sum_{j=1}^{6} \alpha^{(0)}_{j,-2} \sqrt{\frac{2}{j}} e^{-i\bar{\phi}^{(0)}_{j,-2}[F(t_0)]} e^{-i(\Psi^{-2}_j+\pi/4)} + \sum_{j=1}^{4} \alpha^{(0)}_{j,0} \sqrt{\frac{2}{j}} e^{-i\bar{\phi}^{(0)}_{j,0}[F(t_0)]} e^{-i(\Psi^{0}_j+\pi/4)} + \sum_{j=1}^{2} \alpha^{(0)}_{j,+2} \sqrt{\frac{2}{j}} e^{-i\bar{\phi}^{(0)}_{j,+2}[F(t_0)]} e^{-i(\Psi^{+2}_j+\pi/4)} \right\}, \tag{3.14}$$

where we have used the quadrupolar (Newtonian) order differential equation for the orbital frequency, available in Refs. [34,55], to compute the amplitudes of $\tilde{h}[F(t_0)]$. Note that we require employing the earlier defined stationary points to replace $F(t_0)$. In practice, we employ the unperturbed stationary points, namely, $F(t_0) = f/j$, while evaluating the amplitudes of $\tilde{h}(f)$.

In what follows, we collect the above pieces together to display the quadrupolar-order $\tilde{h}(f)$ that incorporates fourth order orbital eccentricity contributions while including the effects due to the 3PN-accurate frequency, eccentricity evolution, and periastron advance as

$$\tilde{h}(f) = \left(\frac{5\pi\eta}{384}\right)^{1/2} \frac{G^2m^2}{c^5 D_L} \left(\frac{Gm\pi f}{c^3}\right)^{-7/6} \times \left\{ \sum_{j=1}^{6} \xi^{(0)}_{j,-2} \left(\frac{j}{2}\right)^{2/3} e^{-i(\Psi^{-2}_j+\frac{\pi}{4})} + \sum_{j=1}^{4} \xi^{(0)}_{j,0} \left(\frac{j}{2}\right)^{2/3} e^{-i(\Psi^{0}_j+\frac{\pi}{4})} + \sum_{j=1}^{2} \xi^{(0)}_{j,+2} \left(\frac{j}{2}\right)^{2/3} e^{-i(\Psi^{+2}_j+\frac{\pi}{4})} \right\}, \tag{3.15}$$

where the Fourier amplitudes $\xi^{(0)}_{j,\pm n}$ are now given by

$$\xi^{(0)}_{j,\pm n} = \frac{(1-e_t^2)^{7/4}}{(1+\frac{73}{24}e_t^2+\frac{37}{96}e_t^4)^{1/2}} \alpha^{(0)}_{j,\pm n} e^{-i\bar{\phi}^{(0)}_{j,\pm n}(f/j)}, \tag{3.16}$$

and n takes values 0 and 2. A crucial expression that will be required to operationalize the above $\tilde{h}(f)$, namely, the 3PN-accurate expression for e_t in terms of e_0, x, and χ, is listed as Eq. (C1) in Appendix C. Note that the approach to obtain such an expression for e_t is detailed in Ref. [49] and briefly summarized in Sec. II A. Finally, the fully 3PN-accurate expression for $\Psi^n_j(f)$ that incorporates fourth order orbital eccentricity contributions at each PN order is displayed as Eq. (C5) in Appendix C. It should be noted that the approach of SPA demands the evaluation of Fourier amplitudes, $\xi_{j,\pm n}$ and Fourier phases, $\Psi^{\pm n}_j$ at $F(t^{\pm n}) = f/(j-(j\pm n)k^{(6)}_{(3)})$.

We have extended these calculations by including 1PN-accurate amplitude corrections to $h_\times$ and h_+ with the help of Eqs. (2.27), (2.28a), (2.28b), and (2.28c). Additionally, we have included initial eccentricity corrections, accurate to $\mathcal{O}(e_0^6)$, in our 3PN-accurate e_t and $\Psi^n_j(f)$ expressions. We note in passing that these expressions are available in the accompanying Mathematica file [65]. The resulting expression for $\tilde{h}(f)$ may be symbolically written as

$$\tilde{h}(f) = \left(\frac{5\pi\eta}{384}\right)^{1/2} \frac{G^2m^2}{c^5 D_L} \left(\frac{Gm\pi f}{c^3}\right)^{-7/6} \left\{ \left[\sum_{j=1}^{6} \xi^{(0)}_{j,0} \left(\frac{j}{2}\right)^{2/3} e^{-i(\Psi^{0}_j+\frac{\pi}{4})} + \sum_{j=1}^{4} \xi^{(0)}_{j,+2} \left(\frac{j}{2}\right)^{2/3} e^{-i(\Psi^{+2}_j+\frac{\pi}{4})} + \sum_{j=1}^{8} \xi^{(0)}_{j,-2} \left(\frac{j}{2}\right)^{2/3} e^{-i(\Psi^{-2}_j+\frac{\pi}{4})} \right] + \left(\frac{Gm\pi f}{c^3}\right)^{1/3} \delta \left[\sum_{j=1}^{5} \xi^{(0.5)}_{j,+1} \left(\frac{j}{2}\right)^{1/3} e^{-i(\Psi^{+1}_j+\frac{\pi}{4})} + \sum_{j=1}^{7} \xi^{(0.5)}_{j,-1} \left(\frac{j}{2}\right)^{1/3} e^{-i(\Psi^{-1}_j+\frac{\pi}{4})} + \sum_{j=1}^{3} \xi^{(0.5)}_{j,+3} \left(\frac{j}{2}\right)^{1/3} e^{-i(\Psi^{+3}_j+\frac{\pi}{4})} + \sum_{j=1}^{9} \xi^{(0.5)}_{j,-3} \left(\frac{j}{2}\right)^{1/3} e^{-i(\Psi^{-3}_j+\frac{\pi}{4})} \right] + \left(\frac{Gm\pi f}{c^3}\right)^{2/3} \left[\sum_{j=1}^{6} \xi^{(1)}_{j,0} e^{-i(\Psi^{0}_j+\frac{\pi}{4})} + \sum_{j=1}^{4} \xi^{(1)}_{j,+2} e^{-i(\Psi^{+2}_j+\frac{\pi}{4})} + \sum_{j=1}^{8} \xi^{(1)}_{j,-2} e^{-i(\Psi^{-2}_j+\frac{\pi}{4})} + \sum_{j=1}^{2} \xi^{(1)}_{j,+4} e^{-i(\Psi^{+4}_j+\frac{\pi}{4})} + \sum_{j=1}^{10} \xi^{(1)}_{j,-4} e^{-i(\Psi^{-4}_j+\frac{\pi}{4})} \right] \right\}. \tag{3.17}$$

In the above expression, the Fourier amplitudes are given by

$$\xi^{(p)}_{j,\pm n} = \Bigg\{ \frac{(1-e_t^2)^{7/4}}{(1+\frac{73}{24}e_t^2+\frac{37}{96}e_t^4)^{1/2}} + \frac{(1-e_t^2)^{3/4}}{10752(1+\frac{73}{24}e_t^2+\frac{37}{96}e_t^4)^{3/2}}[11888+14784\eta - e_t^2(87720-159600\eta) - e_t^4(171038-141708\eta) - e_t^6(11717-8288\eta)] \Bigg\} \alpha^{(p)}_{j,\pm n} e^{-i\bar{\phi}^{(p)}_{j,\pm n}}, \tag{3.18}$$

where the superscript p takes values 0, 0.5, and 1 in our amplitude-corrected $\tilde{h}(f)$. Further, we have used the 1PN-accurate differential equation for the orbital frequency while obtaining the Fourier amplitude expressions. This expression, adaptable from Eqs. (B8a) and (B9a) of Ref. [49], reads

$$\frac{dF}{dt} = \frac{48c^6\eta}{5\pi G^2 m^2}\left(\frac{Gm2\pi F}{c^3}\right)^{11/3}\frac{(1+\frac{73}{24}e_t^2+\frac{37}{96}e_t^4)}{(1-e_t^2)^{7/2}} - \frac{743c^6\eta}{35\pi G^2m^2}\left(\frac{Gm2\pi F}{c^3}\right)^{13/3}\frac{1}{(1-e_t^2)^{9/2}} \times\left\{1+\frac{924}{743}\eta+e_t^2\left(-\frac{10965}{1486}+\frac{9975}{743}\eta\right)+e_t^4\left(-\frac{85519}{5944}+\frac{35427}{2972}\eta\right)+e_t^6\left(-\frac{11717}{11888}+\frac{518}{743}\eta\right)\right\}. \tag{3.19}$$

The explicit expressions for e_t and $\Psi^n_j(f)$ that incorporate the next-to-leading-order e_0 corrections at each PN order, as noted earlier, are listed in the Appendix C.

We move on to contrast our approach with other attempts in the literature. Section VI of Ref. [44] indeed sketched a road map to include PN corrections to their Newtonian waveform family. This road map included a suggestion to incorporate the effect of the periastron advance into their quadrupolar-order GW polarization states, influenced by Ref. [34]. Their suggestion involves splitting the orbital phase evolution into two parts where one part remains linear in the mean anomaly l while the other part is periodic in l. These considerations influenced them to rewrite our Eq. (2.3) essentially to be

$$h(t) = -\frac{Gm\eta}{c^2 D_L} x \sum_{j=1}^{10} \alpha_j \cos\{jl(1+k^{(6)}_{(1)}) + \phi_j\}, \tag{3.20}$$

where $k^{(6)}_{(1)}$ stands for the 1PN-accurate expression for k, given by $3x/(1-e_t^2)$, expanded to the sixth order in e_t [see our Eq. (3.10)]. It is not difficult to see that the associated SPA based Fourier phase takes the following form:

$$\Psi_j(F) = \lambda[t(f/j)] - 2\pi f t(f/j), \tag{3.21}$$

where

$$\lambda[t(f/j)] = j\phi_c + j\int^{f/j}\frac{\dot{\lambda}'}{\dot{F}'}dF' \tag{3.22}$$

$$t(f/j) = t_c + \int^{f/j}\frac{dF'}{\dot{F}'}. \tag{3.23}$$

It turned out that $\dot{\lambda}' \equiv \omega$ by construction. The use of ω in the above Fourier phase expression essentially ensures that the suggestion of Ref. [44] leads to what is detailed in Ref. [49]. Note that Ref. [49] provided $\tilde{h}(f)$ in terms of an infinite set of harmonics with quadrupolar-order amplitudes and the 2PN-accurate Fourier phase. We observe that Ref. [44] indeed commented on the absence of side bands in their prescription in comparison with what was reported in Refs. [67,68] and suggested future investigations to clarify the issue. In contrast, the present investigation employs Eq. (2.32), which explicitly incorporates the effect of the periastron advance both in the amplitude and phase of GW polarization states, as detailed in Ref. [45]. The use of such an expression ensures that our analytic Fourier domain expression does indeed contain the periastron advance induced frequency side bands. Additionally, Refs. [29,59] employed the dominant order periastron advance induced decomposition of Fourier phases, associated with the quadrupolar-order gravitational waveform, while exploring LISA and aLIGO relevant parameter estimation studies. A close comparison of Eqs. (B10) and (B11) of Ref. [59] and Eqs. (35) and (36) of Ref. [29] with our Eq. (3.10) reveals fairly identical expressions for the Fourier phases. These considerations allowed us to state that our expression for $\tilde{h}(f)$, given by Eqs. (3.17), (3.18), (C1), and (C5), provides analytic PN-accurate Fourier domain templates for compact binaries inspiraling along PN-accurate precessing eccentric orbits. We are now in a position to explore basic GW data analysis implications of our inspiral templates.

B. Preliminary GW data analysis implications

We employ the familiar match computations to probe basic GW data analysis implications of our PN-accurate

inspiral templates. Following Ref. [52], the match $\mathcal{M}(h_s, h_t)$ between members of two waveform classes, namely, signal h_s and template h_t, is computed by maximizing a certain overlap integral $\mathcal{O}(h_s, h_t)$ with respect to the kinematic variables of the template waveform. In other words,

$$\mathcal{M}(h_s, h_t) = \max_{t_0,\phi_0} \mathcal{O}(h_s, h_t), \tag{3.24}$$

where t_0 and ϕ_0 are the detector arrival time and the associated arrival phase of our template. The overlap integral involves the interferometer-specific normalized inner product between members of the h_s and h_t families; it reads

$$\langle h_s|h_t\rangle = 4\mathrm{Re}\int_{f_{\rm low}}^{f_{\rm high}} \frac{\tilde{h}_s^*(f)\tilde{h}_t(f)}{S_{\rm h}(f)}\,df, \tag{3.25}$$

where $\tilde{h}_s(f)$ and $\tilde{h}_t(f)$ are the Fourier transforms of the $h_s(t)$ and $h_t(t)$ inspiral waveforms. Further, $S_{\rm h}(f)$ denotes the one-sided power spectral density of the detector noise. In the following, we employ the zero-detuned, high power (ZDHP) noise configuration of Advanced LIGO at design sensitivity [69]. In our $\mathcal{M}$ estimates, we let $f_{\rm low}$ be 20 Hz, corresponding to the lower cutoff frequency of Advanced LIGO. The upper frequency limit $f_{\rm high}$ is chosen to be the usual $f_{\rm LSO} = c^3/(Gm\pi 6^{3/2})$ of the last stable circular orbit. We have verified that orbital eccentricities of compact binaries reduce to well below 10^{-2} at $f_{\rm high} = f_{\rm LSO}$, thereby justifying the use of the last stable circular orbit frequency for the upper frequency limit.

We require additional steps to operationalize our inspiral templates while performing the $\mathcal{M}$ computations. Clearly, these waveform families should only be implemented within the physically allowed frequency intervals. This is to ensure that the many higher harmonics present in these waveform families do not cross the above listed upper frequency limit. Influenced by Ref. [44], we invoke the *unit step function* (Θ) to operationalize our inspiral templates. This step function allows us to appropriately terminate the waveform as $\Theta(y) = 1$ for $y \geq 0$ and *zero* otherwise. The structure of our quadrupolar amplitude inspiral family, given by Eq. (3.15), compels us to invoke Θ functions such that

$$\begin{aligned}\tilde{h}(f) = \left(\frac{5\pi\eta}{384}\right)^{1/2}\frac{G^2m^2}{c^5D_L}\left(\frac{Gm\pi f}{c^3}\right)^{-7/6}\Bigg\{&\sum_{j=1}^{4}\xi^{(0)}_{j,0}\left(\frac{j}{2}\right)^{2/3}e^{-i(\frac{\pi}{4}+\Psi^0_j)}\times\Theta[(j-jk^{(6)}_{(3)})f_{\rm LSO}-2f]\\&+\sum_{j=1}^{2}\xi^{(0)}_{j,+2}\left(\frac{j}{2}\right)^{2/3}e^{-i(\frac{\pi}{4}+\Psi^{+2}_j)}\times\Theta[(j-(j+2)k^{(6)}_{(3)})f_{\rm LSO}-2f]+\sum_{j=1}^{6}\xi^{(0)}_{j,-2}\left(\frac{j}{2}\right)^{2/3}e^{-i(\frac{\pi}{4}+\Psi^{-2}_j)}\\&\times\Theta[(j-(j-2)k^{(6)}_{(3)})f_{\rm LSO}-2f]\Bigg\}.\end{aligned} \tag{3.26}$$

Note that we have appropriately shifted the upper frequency limits to ensure that higher *harmonics* are suitably terminated. While implementing our $\tilde{h}(f)$ we have encountered the violation of the stationary phase condition, namely Eq. (3.11), at a few Fourier frequencies corresponding to lower harmonic indices ($j \sim 1, 2$). We infer that the periastron advance induced shift of these harmonics can lead to negative GW frequencies. Therefore, we have discarded such Fourier components. Interestingly, Ref. [46] showed that these harmonics provide negligible contributions to the GW power spectrum, which may be used to justify our neglect of such Fourier components in the implementation of our waveform families. The above steps ensure smoothly varying templates which we will use in the following to pursue match computations. We provide three frequency series of the same length (corresponding to h_s and h_t inspiral families and the ZDHP noise power spectral density) and employ a routine from the free and open software package PyCBC [70] to compute various $\mathcal{M}$ estimates.

We qualify the implications of our match estimates on GW data analysis by considering the threshold $\mathcal{M}(h_s,h_t) \geq 0.97$, denoted in the presentation of results in Figs. 1–3 by solid black lines. This limit corresponds to a loss of less than 10% of all signals in the matched filter searches. In regions of parameter space where the computed matches are high, i.e., $\mathcal{M} \geq 0.97$, waveform models are generally considered both *effectual* templates for the detection of fiducial GW signals and reasonably *faithful* in the estimation of GW source parameters [52]. However, even if $\mathcal{M}$ is larger than 0.97, certain errors in the model waveform (due to unmodeled effects of, e.g., eccentricity) may become *distinguishable* from noise at a high signal-to-noise ratio (SNR) and can affect the accuracy of the source parameter estimation. Negligible systematic errors in the parameter estimation—despite differences between the true signal waveform and the template model—can be guaranteed only if $(h_s - h_t, h_s - h_t) < 1$, the so-called *indistinguishability criterion* [71]. In other words, such systematic errors in the estimated source parameters may become significant when

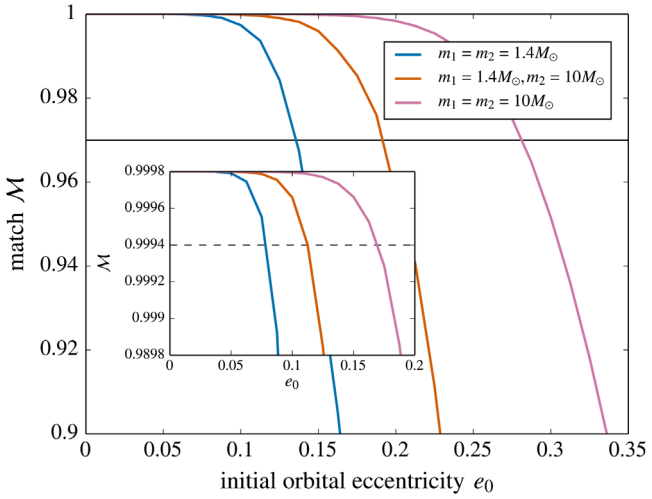

FIG. 1. Matches between eccentric waveform models with different orders of eccentricity corrections. We are comparing waveforms that take only leading-order $\mathcal{O}(e_0^2)$ eccentricity corrections into account to those that include eccentricity corrections up to next-to-next-to leading order $\mathcal{O}(e_0^6)$. We consider three configurations of a NS and a BH with masses of 1.4 $M_\odot$ and 10 $M_\odot$, respectively: i.e., NS-NS (blue curve), NS-BH (orange curve), and BH-BH (pink curve) systems. The initial orbital eccentricity e_0 refers to the eccentricity of the binary system at 20 Hz. Given the same e_0, the effect of higher-order eccentricity corrections on the agreement between signal and template is strongly dependent on the total mass of the compact binary source. The solid black line denotes the threshold $\mathcal{M} = 0.97$, associated with the effectualness of a model for GW detection and its faithfulness for source parameter estimation. The inset plot zooms into the region of parameter space where we can expect the effect of higher-order eccentricity corrections to become distinguishable from noise for SNR = 30, leading to systematic errors in parameter estimation; the dashed black line represents the indistinguishability criterion.

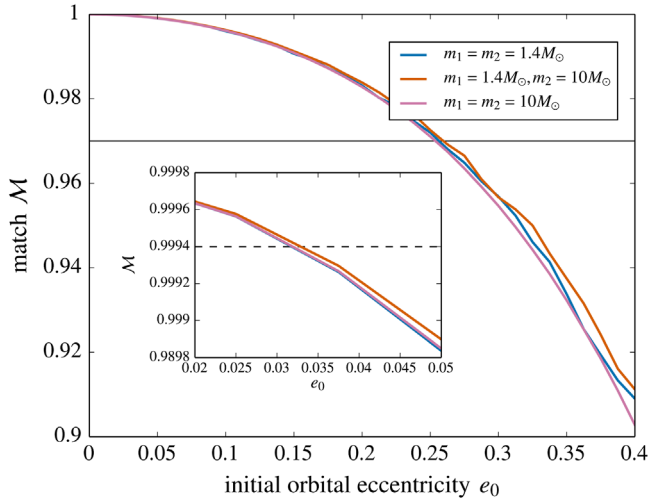

FIG. 2. Matches between eccentric waveform models that include or neglect effects of the periastron advance. We consider the same three configurations of binaries with NS and BH components as in Fig. 1: i.e., NS-NS (blue curve), NS-BH (orange curve), and BH-BH (pink curve) systems. The initial orbital eccentricity e_0 is again defined at the lower cutoff frequency 20 Hz. We infer that the significance of periastron advance effects for GW data analysis is rather independent of the total mass of the source. We interpret our results by considering the threshold $\mathcal{M} = 0.97$ (represented by the solid black line) below which a waveform model should be considered ineffectual for detection and unfaithful for parameter estimation. In the inset plots, we highlight the parameter space of small eccentricities to probe the importance of systematic errors in parameter estimation due to waveform uncertainties. The dashed black line represents the distinguishable limit for a fiducial GW signal with SNR = 30.

they mismatch $1 - \mathcal{M}_c \geq 1/\mathrm{SNR}^2$ and clearly depend on the amplitude of the signal. In the following analysis, we let the signal-to-noise ratio of our fiducial GW signals be SNR = 30 (corresponding to the SNR of the binary neutron star inspiral GW170817) and probe the distinguishability of certain effects in our model waveforms for inspiraling eccentric binaries. In the inset plots of Figs. 1 and 2, we zoom into those regions of parameter space where we can expect waveform uncertainties to become indistinguishable from noise for SNR = 30; the corresponding distinguishable limit $\mathcal{M}_c$ is represented by the dashed black lines.

We first probe the importance of higher-order eccentricity corrections in the GW phasing. For this purpose, we let the signal family h_s be our quadrupolar-order $\tilde{h}(f)$, with a 3PN-accurate Fourier phase that includes next-to-next-to-leading-order $\mathcal{O}(e_0^6)$ eccentricity corrections at each PN order. The template family is given by a quadrupolar-order $\tilde{h}(f)$ in the low-eccentricity limit, incorporating only the leading-order $\mathcal{O}(e_0^2)$ eccentricity contributions in the 3PN-accurate Fourier phase. We consider the traditional nonspinning compact binary sources relevant for Advanced LIGO: namely, binary neutron stars (NS-NS), NS-BH systems, and binary black holes (BH-BH), with NS and BH components of 1.4 $M_\odot$ and 10 $M_\odot$, respectively. For each of these three configurations, we compute the match between signal and template waveforms for different values of the initial orbital eccentricity e_0 between 0 and 0.4 (defined at the cut-off frequency 20 Hz). Figure 1 suggests that the importance of higher-order eccentricity corrections for GW data analysis is strongly dependent on the total mass of an eccentric compact binary source. Given the same e_0 but for configurations with increasing total mass, we find that templates restricted to leading-order eccentricity corrections become increasingly faithful representations of those inspiral waveforms that include higher-order eccentricity effects at each PN order. This is expected, as compact binaries with higher total mass provide a smaller number of inspiral GW cycles in the frequency window of Advanced LIGO. Therefore, these systems require larger initial eccentricities to bring on a substantial dephasing and subsequent mismatch between our inspiral signal and template families. Figure 1 indicates that a waveform

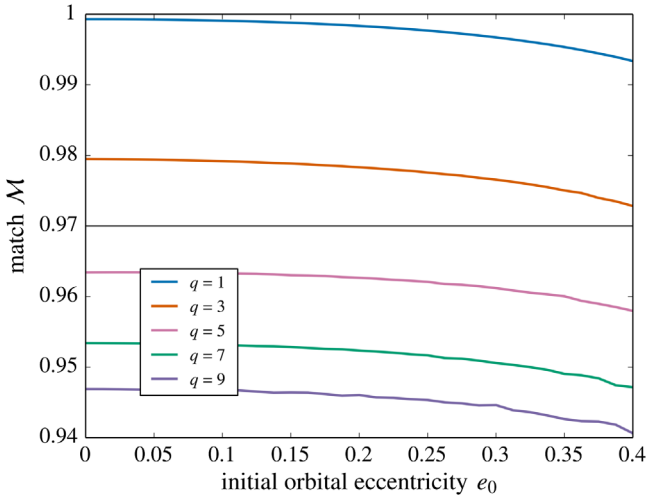

FIG. 3. Matches between eccentric waveform models with Newtonian and 1PN-accurate amplitudes. We consider compact binary systems with a total mass of $m = m_1 + m_2$, with different choices for the mass ratio $q = m_1/m_2$. As expected, the effect of amplitude corrections on waveform faithfulness is largely independent of the orbital eccentricity e_0 at 20 Hz. Waveforms with Newtonian amplitudes are faithful representations of amplitude-corrected waveforms only if $q \leq 3$ (blue and orange curves); for higher mass ratios $q \geq 5$ (pink, green and purple curves) the match between waveforms with Newtonian and 1PN-accurate amplitudes falls below the threshold of $\mathcal{M} = 0.97$ (denoted by the black line) even in the circular limit.

model restricted to only leading-order eccentricity corrections would be an effectual template family for the detection of GWs from even moderately eccentric inspirals (with $e_0 \leq 0.15$ and ≤ 0.3 for our traditional NS-NS and BH-BH binaries, respectively). However, the inset of Fig. 1 suggests that waveform effects of higher-order eccentricity corrections become distinguishable from detector noise at significantly lower initial eccentricities ($e_0 \geq 0.07$ and ≥ 0.17 for GWs from NS-NS and BH-BH systems with SNR $= 30$). In this region of parameter space, we should expect systematic errors in source parameter estimation with inspiral templates that are accurate only to leading order in eccentricity e_0. The inclusion of higher-order eccentricity corrections in waveform modeling is therefore desirable for an accurate follow-up of eccentric GW signals.

We move on to probe data analysis implications of including the effect of the periastron advance in our eccentric inspiral waveforms $\tilde{h}(f)$. In our match calculation $\mathcal{M}(h_s, h_t)$, the signal waveforms employ our quadrupolar-order $\tilde{h}(f)$ given by Eq. (3.15), including both k and e_t effects to the sixth order in e_0 at each PN order. We build a template family h_t that neglects effects of the periastron advance, by extending to 3PN order previously developed eccentric inspiral waveforms (provided with the 2PN-accurate Fourier phase in Ref. [49]). In other words, we construct quadrupolar templates $\tilde{h}_t(f)$ with the help of Eq. (2.5) and the 3PN extension of our Newtonian equation (2.11) for Ψ_j while incorporating all $\mathcal{O}(e_0^6)$ corrections at each PN order. Additionally, we evaluate the Fourier phase at the unperturbed stationary point $F = f/j$ [44]. It is important to note that such a template waveform family ignores the effect of the periastron advance in its Fourier phase evolution. We consider the same NS-NS, NS-BH, and BH-BH systems as before and compute the match between signal and template waveforms for discrete values of initial orbital eccentricity at 20 Hz, $e_0 \in [0, 0.4]$. From our results, presented in Fig. 2, we learn that the significance of the periastron advance effects for GW data analysis is rather independent of the total mass of the source, with similar match estimates for all three traditional compact binaries under consideration. The periastron advance starts to influence the effectualness of GW templates for detection only for systems that have eccentricities $e_0 > 0.25$ at 20 Hz. This agrees with our observation that k-induced modulations in the inspiral waveforms presented in Fig. 5 and 6 of Ref. [34] become clearly visible only for moderate values of initial orbital eccentricity. However, we can expect systematic biases in the source parameter estimation for much smaller values of orbital eccentricity. The inset of Fig. 2 suggests that the periastron advance effects in an eccentric GW signal with SNR $= 30$ would already become distinguishable from noise for eccentricities $e_0 > 0.03$ at 20 Hz, leading to systematic errors in the recovered source parameters when waveform models neglect the periastron advance.

Lastly, we explore the relevance of PN-accurate amplitude corrections while constructing realistic analytic Fourier domain waveforms for eccentric inspirals. For these $\mathcal{M}$ estimates, we invoke as the expected GW signal our 1PN-accurate amplitude-corrected $\tilde{h}(f)$, given by Eq. (3.17), including the effects of the 3PN-accurate periastron advance, frequency, and eccentricity evolution accurate to sixth order in orbital eccentricity. For the template family, we are utilizing a quadrupolar-order $\tilde{h}(f)$, given by Eq. (3.15), that includes the same order effects of the 3PN-accurate periastron advance and 3PN-accurate frequency and eccentricity evolution as above. We consider five compact binary configurations with a fixed total mass $m = m_1 + m_2 = 20\ M_\odot$ and varying mass ratios $q = m_1/m_2 \in \{1, 3, 5, 7, 9\}$. For each of these configurations, we pursue match computations for different choices of initial orbital eccentricity $e_0 \in [0, 0.4]$ at 20 Hz, resulting in Fig. 3. We observe that amplitude corrections are rather unimportant while constructing template waveforms for equal-mass binaries in eccentric orbits. This is expected, as the dominant amplitude corrections—appearing at 0.5PN order in Eq. (3.17)—are proportional to $\sqrt{1-4\eta}$ and therefore vanish for equal-mass binaries. Our plots suggest that the effect of amplitude corrections on the faithfulness of eccentric inspiral waveforms crucially depends on the mass ratio of a binary system, with $\mathcal{M}$ rapidly dropping

below the critical value of 0.97 as $q \geq 5$, even for systems with negligible initial eccentricities. This is a familiar result from the modeling of compact binary inspiral along circular orbits and points to the relevance of higher modes for GWs from binaries with asymmetric masses [72]. In other words, our plots in Fig. 3 essentially confirm the previous literature that compared restricted and amplitude-corrected $\tilde{h}(f)$ for the quasicircular inspiral. Interestingly, we find that the q-dependent effect of amplitude corrections on the faithfulness of eccentric inspiral waveforms is largely unaffected by the value of the initial eccentricity e_0.

IV. CONCLUSIONS

We have provided fully analytic PN-accurate Fourier domain gravitational waveforms for compact binaries inspiraling along precessing moderately eccentric orbits. Our inspiral approximant contains 1PN-accurate amplitude corrections and its Fourier phase incorporates the effects of the 3PN-accurate periastron advance and GW emission. Additionally, the eccentricity effects are accurate to sixth order in e_0 at each PN order. We infer from our analytic waveform expression that the orbital eccentricity induced higher harmonics are no longer integer multiples of orbital frequency due to the influence of the periastron advance. This substantiates and extends what is detailed in Ref. [45] for compact binaries inspiraling along PN-accurate precessing eccentric orbits. Preliminary GW data analysis implications of our waveforms are probed with the help of the usual match computations.

In what follows, we provide a step-by-step summary of our effort.

(1) We start from our Eqs. (2.18) and (2.19) that provide quadrupolar order GW polarization states from compact binaries in PN-accurate eccentric orbits as a sum over various harmonics.

(2) With the above inputs, we compute the time-domain GW detector response function and express it as a summation of several cosine functions whose arguments are a sum of integer multiples of ϕ and ϕ' associated with the orbital and periastron motions. Amplitudes of these functions are expressed in terms of ω, e_t and the angles that specify the antenna patterns $F_\times$, F_+, and the direction of the orbital angular momentum vector. The quadrupolar version of $h(t)$ that explicitly incorporates the next-to-leading-order e_t corrections is given by Eq. (2.22) and associated expressions like Eqs. (A1) and (A2). Its 1PN extension is symbolically provided by Eq. (2.32) and the accompanying Mathematica file [65] provides the explicit expressions for various PN coefficients while incorporating $\mathcal{O}(e_t^6)$ corrections.

(3) We also provide a prescription to obtain temporally evolving $h(t)$ for compact binaries inspiraling due to 3PN-accurate GW emission along precessing 3PN-accurate orbits of moderate eccentricities. This involves imposing temporal evolution for ω, e_t, ϕ', and ϕ with the help of PN-accurate differential equations. The relative 3PN-accurate equations for ω and e_t are due to the emission of GWs, as evident from our Eqs. (2.25) and (2.26). The conservative 3PN-accurate differential equation for ϕ' arises essentially due to the periastron advance as evident from Eq. (2.24). The differential equation for ϕ is kinematical in nature as $d\phi/dt \equiv \omega$.

(4) The structure of the time-domain response function allows us to involve the method of stationary phase approximation to compute its Fourier transform. The crucial Fourier phases and the associated "nine" stationary points may be concisely written as $\Psi^{\pm n}(t) \coloneqq -2\pi f t + j\phi - (j \pm n)\phi'$, where n takes values 0, 1, 2, 3, 4. The nine stationary points, associated with the 1PN-accurate amplitude-corrected $h(t)$, essentially provide relations between the orbital and Fourier frequencies $F(t^{\pm n}) = f/(j - (j \pm n)k')$, where k' is related to the rate of the periastron advance per orbit. The explicit expression for the resulting 3PN-accurate Fourier phases with leading-order initial eccentricity corrections are provided by Eq. (3.13). Gathering various results, we obtain Eqs. (3.15) and (3.16), which provide the quadrupolar-order $\tilde{h}(f)$ while incorporating fourth order orbital eccentricity contributions along with the effects due to the 3PN-accurate frequency, eccentricity evolution, and periastron advance. Additionally, we have extended these results by including 1PN-accurate amplitude corrections and six order eccentricity contributions.

(5) A crucial ingredient to obtain a fully analytic $\tilde{h}(f)$ involves a derivation, detailed in Sec. II, that provides the PN-accurate analytic expression for e_t in terms of e_0, ω, ω_0. We have obtained the 3PN-accurate expression for $e_t(e_0, \omega, \omega_0)$ by extending the postcircular scheme of Refs. [44,49].

A number of extensions are possible. Influenced by Refs. [73,74], we are incorporating the effects of leading-order aligned spin-orbit and spin-spin interactions into these waveforms. It will be interesting to explore data analysis implications of our present waveforms. A possible avenue is to explore the astrophysical implications of using PN-accurate periastron advance contributions that depend both on m and η, influenced by Refs. [59,75]. There are ongoing efforts to construct analytic IMR templates to model eccentric compact binary coalescence [19,37]. The present waveform family will be relevant to construct IMR templates for moderately eccentric compact binary mergers which can be used to extract orbital eccentricity and the periastron advance as done in Ref. [76]. Efforts are ongoing to obtain various constructs, using elements of our postcircular Fourier domain approximant, that should allow us to make comparisons with a brand new PN-accurate

frequency domain waveform family, developed in Refs. [58,77] for moderate eccentricities.

ACKNOWLEDGMENTS

We thank Yannick Boetzel for helpful discussions, suggestions, and for providing us with the lengthy eccentricity enhancement functions. We are grateful to Marc Favata and Blake Moore for their helpful comments. M. H. acknowledges support from Swiss National Science Foundation (SNSF) Grant No. IZCOZ0_177057. We have used software packages from PyCBC [70] and Matplotlib [78] to compute and plot match estimates.

APPENDIX A: $\Gamma^{(0)}_{j,\pm n}$ AND $\Sigma^{(0)}_{j,\pm n}$ COEFFICIENTS

We list the $\Gamma^{(0)}_{j,\pm n}$ and $\Sigma^{(0)}_{j,\pm n}$ coefficients appearing in Eq. (2.21). The relevant $\Gamma^{(0)}_{j,\pm n}$ expressions read

$$\Gamma^{(0)}_{1,-2} = F_+\left\{\left(\frac{3e_t}{2}-\frac{13e_t^3}{16}\right)(1+c_i^2)c_{2\beta}\right\} + F_\times\left\{\left(-3e_t+\frac{13e_t^3}{8}\right)c_i s_{2\beta}\right\}, \tag{A1a}$$

$$\Gamma^{(0)}_{2,-2} = F_+\left\{\left(-2+5e_t^2-\frac{23e_t^4}{8}\right)(1+c_i^2)c_{2\beta}\right\} + F_\times\left\{\left(4-10e_t^2+\frac{23e_t^4}{4}\right)c_i s_{2\beta}\right\}, \tag{A1b}$$

$$\Gamma^{(0)}_{3,-2} = F_+\left\{\left(-\frac{9e_t}{2}+\frac{171e_t^3}{16}\right)(1+c_i^2)c_{2\beta}\right\} + F_\times\left\{\left(9e_t-\frac{171e_t^3}{8}\right)c_i s_{2\beta}\right\}, \tag{A1c}$$

$$\Gamma^{(0)}_{4,-2} = F_+\{(-8e_t^2+20e_t^4)(1+c_i^2)c_{2\beta}\} + F_\times\{(16e_t^2-40e_t^4)c_i s_{2\beta}\}, \tag{A1d}$$

$$\Gamma^{(0)}_{5,-2} = F_+\left\{-\frac{625}{48}e_t^3(1+c_i^2)c_{2\beta}\right\} + F_\times\left\{\frac{625}{24}e_t^3 c_i s_{2\beta}\right\}, \tag{A1e}$$

$$\Gamma^{(0)}_{6,-2} = F_+\left\{-\frac{81}{4}e_t^4(1+c_i^2)c_{2\beta}\right\} + F_\times\left\{\frac{81}{2}e_t^4 c_i s_{2\beta}\right\}, \tag{A1f}$$

$$\Gamma^{(0)}_{1,0} = F_+\left\{\left(e_t-\frac{e_t^3}{8}\right)s_i^2\right\}, \tag{A1g}$$

$$\Gamma^{(0)}_{2,0} = F_+\left\{\left(e_t^2-\frac{e_t^4}{3}\right)s_i^2\right\}, \tag{A1h}$$

$$\Gamma^{(0)}_{3,0} = F_+\left\{\frac{9}{8}e_t^3 s_i^2\right\}, \tag{A1i}$$

$$\Gamma^{(0)}_{4,0} = F_+\left\{\frac{4}{3}e_t^4 s_i^2\right\}, \tag{A1j}$$

$$\Gamma^{(0)}_{1,+2} = F_+\left\{\frac{7}{48}e_t^3(1+c_i^2)c_{2\beta}\right\} + F_\times\left\{-\frac{7}{24}e_t^3 c_i s_{2\beta}\right\}, \tag{A1k}$$

$$\Gamma^{(0)}_{2,+2} = F_+\left\{-\frac{1}{8}e_t^4(1+c_i^2)c_{2\beta}\right\} + F_\times\left\{-\frac{1}{4}e_t^4 c_i s_{2\beta}\right\}. \tag{A1l}$$

The $\Sigma^{(0)}_{j,\pm n}$ counterparts of the above expressions read

$$\Sigma^{(0)}_{1,-2} = F_+\left\{\left(\frac{3e_t}{2}-\frac{13e_t^3}{16}\right)(1+c_i^2)s_{2\beta}\right\} + F_\times\left\{\left(3e_t-\frac{13e_t^3}{8}\right)c_i c_{2\beta}\right\}, \tag{A2a}$$

$$\Sigma^{(0)}_{2,-2} = F_+\left\{\left(-2+5e_t^2-\frac{23e_t^4}{8}\right)(1+c_i^2)s_{2\beta}\right\} + F_\times\left\{\left(-4+10e_t^2-\frac{23e_t^4}{4}\right)c_i c_{2\beta}\right\}, \tag{A2b}$$

$$\Sigma^{(0)}_{3,-2} = F_+\left\{\left(-\frac{9e_t}{2}+\frac{171e_t^3}{16}\right)(1+c_i^2)s_{2\beta}\right\} + F_\times\left\{\left(-9e_t+\frac{171e_t^3}{8}\right)c_i c_{2\beta}\right\}, \tag{A2c}$$

$$\Sigma^{(0)}_{4,-2} = F_+\{(-8e_t^2+20e_t^4)(1+c_i^2)s_{2\beta}\} + F_\times\{(-16e_t^2+40e_t^4)c_i c_{2\beta}\}, \tag{A2d}$$

$$\Sigma^{(0)}_{5,-2} = F_+\left\{-\frac{625}{48}e_t^3(1+c_i^2)s_{2\beta}\right\} + F_\times\left\{-\frac{625}{24}e_t^3 c_i c_{2\beta}\right\}, \tag{A2e}$$

$$\Sigma^{(0)}_{6,-2} = F_+\left\{-\frac{81}{4}e_t^4(1+c_i^2)s_{2\beta}\right\} + F_\times\left\{-\frac{81}{2}e_t^4 c_i c_{2\beta}\right\}, \tag{A2f}$$

$$\Sigma^{(0)}_{1,0} = 0, \tag{A2g}$$

$$\Sigma^{(0)}_{2,0} = 0, \tag{A2h}$$

$$\Sigma^{(0)}_{3,0} = 0, \tag{A2i}$$

$$\Sigma^{(0)}_{4,0} = 0, \tag{A2j}$$

$$\Sigma^{(0)}_{1,+2} = F_+\left\{-\frac{7}{48}e_t^3(1+c_i^2)s_{2\beta}\right\} + F_\times\left\{-\frac{7}{24}e_t^3 c_i c_{2\beta}\right\}, \tag{A2k}$$

$$\Sigma^{(0)}_{2,+2} = F_+\left\{-\frac{1}{8}e_t^4(1+c_i^2)s_{2\beta}\right\} + F_\times\left\{-\frac{1}{4}e_t^4 c_i c_{2\beta}\right\}. \tag{A2l}$$

APPENDIX B: 3PN-ACCURATE $\frac{d\omega}{dt}$ AND $\frac{de_t}{dt}$

We give here the 3PN-accurate expressions for the temporal evolution of ω and e_t for obtaining $h(t)$ associated with compact binaries inspiraling along precessing eccentric orbits. 1PN-accurate $\frac{d\omega}{dt}$ and $\frac{de_t}{dt}$ with $\mathcal{O}(e_t^6)$ eccentricity corrections are given by Eq. (2.25) and Eq. (2.26), respectively. The 1.5PN–3PN contributions to $\frac{d\omega}{dt}$ appearing in Eq. (2.25) with $\mathcal{O}(e_t^6)$ corrections are

$$\dot{\omega}^{1.5PN} = \pi x^{3/2}\left\{4 + \frac{2335}{48}e_t^2 + \frac{42955}{192}e_t^4 + \frac{6204647}{9216}e_t^6\right\}, \tag{B1a}$$

$$\dot{\omega}^{2PN} = x^2\left\{\frac{34103}{18144} + \frac{13661}{2016}\eta + \frac{59}{18}\eta^2 + \left(-\frac{479959}{12096} + \frac{80425}{4032}\eta + \frac{213539}{1728}\eta^2\right)e_t^2 + \left(-\frac{2932261}{16128} - \frac{5715083}{16128}\eta + \frac{2133235}{2304}\eta^2\right)e_t^4 + \left(-\frac{19581787}{48384} - \frac{1753627}{768}\eta + \frac{25727065}{6912}\eta^2\right)e_t^6\right\}, \tag{B1b}$$

$$\dot{\omega}^{2.5PN} = \pi x^{5/2}\left\{-\frac{4159}{672} - \frac{189}{8}\eta + \left(\frac{7885}{96} - \frac{27645}{56}\eta\right)e_t^2 + \left(\frac{44644883}{43008} - \frac{11707809}{3584}\eta\right)e_t^4 + \left(\frac{971752501}{193536} - \frac{103819241}{8064}\eta\right)e_t^6\right\}, \tag{B1c}$$

$$\begin{aligned}\dot{\omega}^{3PN} = x^3\Bigg\{&\frac{16447322263}{139708800} + \frac{16\pi^2}{3} - \frac{1712\gamma}{105} + \left(-\frac{56198689}{217728} + \frac{451\pi^2}{48}\right)\eta + \frac{541}{896}\eta^2 - \frac{5605}{2592}\eta^3 - \frac{3424\log(2)}{105} \\ &- \frac{856\log(x)}{105} + \left(\frac{277391496167}{139708800} + \frac{992\pi^2}{9} - \frac{106144\gamma}{315} + \left(-\frac{280153957}{120960} + \frac{188231\pi^2}{2304}\right)\eta - \frac{73109}{448}\eta^2\right. \\ &\left. - \frac{6874115}{31104}\eta^3 - \frac{80464\log(2)}{315} - \frac{234009\log(3)}{560} - \frac{53072\log(x)}{315}\right)e_t^2 + \left(\frac{974308007423}{79833600} + \frac{3059\pi^2}{4} - \frac{46759\gamma}{20}\right. \\ &+ \left(-\frac{33126017}{3780} + \frac{2065129\pi^2}{6144}\right)\eta - \frac{2804209}{32256}\eta^2 - \frac{114255295}{41472}\eta^3 - \frac{2730533\log(2)}{252} + \frac{4446171\log(3)}{2240} \\ &\left. - \frac{46759\log(x)}{40}\right)e_t^4 + \left(\frac{150878591021}{3193344} + \frac{76615\pi^2}{24} - \frac{234223\gamma}{24} + \left(-\frac{7739324653}{362880} + \frac{34978699\pi^2}{36864}\right)\eta\right. \\ &+ \frac{21116263}{4608}\eta^2 - \frac{1935750565}{124416}\eta^3 + \frac{80906873\log(2)}{2520} - \frac{134711181\log(3)}{35840} - \frac{5224609375\log(5)}{193536} \\ &\left. - \frac{234223\log(x)}{48}\right)e_t^6\Bigg\},\end{aligned} \tag{B1d}$$

where γ stands for the Euler-Mascheroni constant. The 1.5PN–3PN contributions to $\frac{de_t}{dt}$ appearing in Eq. (2.26) with $\mathcal{O}(e_t^6)$ corrections are

$$\dot{e}_t^{1.5PN} = \pi x^{3/2}\left\{\frac{985}{152} + \frac{21729}{608}e_t^2 + \frac{3061465}{29184}e_t^4 + \frac{161865935}{700416}e_t^6\right\}, \tag{B2a}$$

$$\dot{e}_t^{2PN} = x^2\left\{-\frac{108197}{38304}+\frac{56407}{4256}\eta+\frac{141}{19}\eta^2+\left(-\frac{1368625}{51072}-\frac{288209}{17024}\eta+\frac{274515}{2432}\eta^2\right)e_t^2+\left(-\frac{15037865}{306432}-\frac{30369109}{102144}\eta+\frac{7578425}{14592}\eta^2\right)e_t^4+\left(-\frac{13488023}{408576}-\frac{65394101}{58368}\eta+\frac{87633595}{58368}\eta^2\right)e_t^6\right\}, \tag{B2b}$$

$$\dot{e}_t^{2.5PN} = \pi x^{5/2}\left\{-\frac{55691}{4256}-\frac{19067}{399}\eta+\left(\frac{286789}{3584}-\frac{7810371}{17024}\eta\right)e_t^2+\left(\frac{535570255}{817152}-\frac{31241795}{16128}\eta\right)e_t^4+\left(\frac{92235604259}{39223296}-\frac{164170915723}{29417472}\eta\right)e_t^6\right\}, \tag{B2c}$$

$$\begin{aligned}\dot{e}_t^{3PN} = x^3\Bigg\{&\frac{246060953209}{884822400}+\frac{769\pi^2}{57}-\frac{82283\gamma}{1995}+\left(-\frac{613139897}{2298240}+\frac{22345\pi^2}{3648}\right)\eta-\frac{1046329}{51072}\eta^2-\frac{305005}{49248}\eta^3\\&-\frac{11021\log(2)}{285}-\frac{234009\log(3)}{5320}-\frac{82283\log(x)}{3990}+\left(\frac{1316189396351}{589881600}+\frac{14023\pi^2}{114}-\frac{1500461\gamma}{3990}\right.\\&+\left(-\frac{5882746699}{4596480}+\frac{46453\pi^2}{1536}\right)\eta-\frac{554719}{4788}\eta^2-\frac{100330729}{393984}\eta^3-\frac{2271503\log(2)}{1330}+\frac{6318243\log(3)}{21280}\\&\left.-\frac{1500461\log(x)}{7980}\right)e_t^2+\left(\frac{1499268531223}{168537600}+\frac{10129\pi^2}{19}-\frac{154829\gamma}{95}+\left(-\frac{543123237}{170240}+\frac{2360575\pi^2}{29184}\right)\eta\right.\\&+\frac{36456205}{87552}\eta^2-\frac{1523467085}{787968}\eta^3+\frac{41683669\log(2)}{5985}-\frac{281044809\log(3)}{340480}-\frac{1044921875\log(5)}{204288}\\&\left.-\frac{154829\log(x)}{190}\right)e_t^4+\left(\frac{682257052877}{26966016}+\frac{976185\pi^2}{608}-\frac{2984337\gamma}{608}+\left(-\frac{4722976831}{875520}+\frac{24558057\pi^2}{155648}\right)\eta\right.\\&+\frac{1312493803}{350208}\eta^2-\frac{24620050735}{3151872}\eta^3-\frac{10971071339\log(2)}{191520}-\frac{74286859077\log(3)}{2723840}+\frac{24033203125\log(5)}{700416}\\&\left.-\frac{2984337\log(x)}{1216}\right)e_t^6\Bigg\}.\end{aligned} \tag{B2d}$$

APPENDIX C: 3PN-ACCURATE ANALYTIC EXPRESSIONS FOR e_t AND $\Psi_j^{\pm n}$

We display explicit expressions for 3PN-accurate e_t and Fourier phases that incorporate next-to-leading order e_0 corrections at each PN order. These expressions, along with Eqs. (3.15), (3.16), (2.31), (A1), and (A2), are required to make operational the fully analytic frequency domain quadrupolar-order GW response function for eccentric inspirals that includes $\mathcal{O}(e_0^4)$ corrections at every PN order. We begin by listing explicit expressions for the 3PN-accurate e_t in terms of e_0, χ, and x. The underlying computation is detailed in Ref. [49] and requires 3PN-accurate expressions for $\dot{\omega}$ and $\dot{e}_t$, given by Eqs. (2.25) and (2.26). The fully 3PN-accurate e_t expression that accounts for all the $\mathcal{O}(e_0^3)$ contributions read

$$e_t = \sum_{m=0}^{6}\mathcal{E}_m x^{m/2}. \tag{C1}$$

The coefficients $\mathcal{E}_m$ with next-to-leading order eccentricity corrections $\mathcal{O}(e_0^3)$ at each PN order can be listed as

$$\mathcal{E}_0 = e_0\chi^{-19/18}+\frac{3323}{1824}(\chi^{-19/18}-\chi^{-19/6})e_0^3, \tag{C2a}$$

$$\mathcal{E}_1 = 0, \tag{C2b}$$

$$\mathcal{E}_2 = \left\{\left(-\frac{2833}{2016}+\frac{197\eta}{72}\right)\chi^{-19/18} + \left(\frac{2833}{2016}-\frac{197\eta}{72}\right)\chi^{-31/18}\right\}e_0 + \left\{\left(-\frac{9414059}{3677184}+\frac{654631\eta}{131328}\right)\chi^{-19/18} + \left(\frac{386822573}{47803392}-\frac{1482433\eta}{131328}\right)\chi^{-31/18} + \left(\frac{11412055}{5311488}-\frac{378697\eta}{43776}\right)\chi^{-19/6} + \left(-\frac{9414059}{1225728}+\frac{654631\eta}{43776}\right)\chi^{-23/6}\right\}e_0^3, \tag{C2c}$$

$$\mathcal{E}_3 = \left\{\frac{377}{144}\pi(-\chi^{-19/18}+\chi^{-37/18})\right\}e_0 + \left\{-\frac{1252771\pi}{262656}\chi^{-19/18} + \frac{1315151\pi}{131328}\chi^{-37/18} + \frac{396797\pi}{43776}\chi^{-19/6} - \frac{1252771\pi}{87552}\chi^{-25/6}\right\}e_0^3, \tag{C2d}$$

$$\mathcal{E}_4 = \left\{\left(\frac{77006005}{24385536}-\frac{1143767\eta}{145152}+\frac{43807\eta^2}{10368}\right)\chi^{-19/18} + \left(-\frac{8025889}{4064256}+\frac{558101\eta}{72576}-\frac{38809\eta^2}{5184}\right)\chi^{-31/18} + \left(-\frac{28850671}{24385536}+\frac{27565\eta}{145152}+\frac{33811\eta^2}{10368}\right)\chi^{-43/18}\right\}e_0 + \left\{\left(\frac{255890954615}{44479217664}-\frac{3800737741\eta}{264757248} + \frac{145570661\eta^2}{18911232}\right)\chi^{-19/18} + \left(-\frac{1095868349309}{96371638272}+\frac{65400285919\eta}{1720922112}-\frac{292039301\eta^2}{9455616}\right)\chi^{-31/18} + \left(-\frac{20952382669619}{4047608807424}-\frac{385200824731\eta}{24092909568}+\frac{4301644427\eta^2}{132378624}\right)\chi^{-43/18} + \left(\frac{8180980796033}{1349202935808} + \frac{14604819923\eta}{2676989952}-\frac{317361763\eta^2}{14708736}\right)\chi^{-19/6} + \left(\frac{32330351815}{3569319936}-\frac{10345778159\eta}{191213568}+\frac{74603309\eta^2}{1050624}\right)\chi^{-23/6} + \left(-\frac{9164199307}{2118057984}+\frac{1205846917\eta}{29417472}-\frac{13714021\eta^2}{233472}\right)\chi^{-9/2}\right\}e_0^3, \tag{C2e}$$

$$\mathcal{E}_5 = \left\{\left(\frac{9901567\pi}{1451520}-\frac{202589\pi\eta}{362880}\right)\chi^{-19/18} + \left(-\frac{1068041\pi}{290304}+\frac{74269\pi\eta}{10368}\right)\chi^{-31/18} + \left(-\frac{1068041\pi}{290304} + \frac{74269\pi\eta}{10368}\right)\chi^{-37/18} + \left(\frac{778843\pi}{1451520}-\frac{4996241\pi\eta}{362880}\right)\chi^{-49/18}\right\}e_0 + \left\{\left(\frac{32902907141\pi}{2647572480} - \frac{673203247\pi\eta}{661893120}\right)\chi^{-19/18} + \left(-\frac{11217854617\pi}{529514496}+\frac{558877241\pi\eta}{18911232}\right)\chi^{-31/18} + \left(-\frac{3725822783\pi}{264757248} + \frac{259084747\pi\eta}{9455616}\right)\chi^{-37/18} + \left(\frac{195499289159\pi}{2647572480}-\frac{65776041763\pi\eta}{661893120}\right)\chi^{-49/18} + \left(-\frac{2057616403\pi}{32686080} + \frac{2370731599\pi\eta}{73543680}\right)\chi^{-19/6} + \left(\frac{1124125901\pi}{29417472}-\frac{78169009\pi\eta}{1050624}\right)\chi^{-23/6} + \left(\frac{330949595\pi}{19611648} - \frac{142768769\pi\eta}{2101248}\right)\chi^{-25/6} + \left(-\frac{12693032573\pi}{294174720}+\frac{11292740311\pi\eta}{73543680}\right)\chi^{-29/6}\right\}e_0^3. \tag{C2f}$$

Because of the lengthy nature of the 3PN order terms in e_t, we split it in two parts as

$$\mathcal{E}_6 = \mathcal{E}_6' e_0 + \mathcal{E}_6'' e_0^3. \tag{C3}$$

The explicit form of these two contributions are

$$\mathcal{E}'_6 = \left(-\frac{33320661414619}{386266890240}+\frac{180721\pi^2}{41472}+\frac{3317\gamma}{252}+\left(\frac{161339510737}{8778792960}+\frac{3977\pi^2}{2304}\right)\eta-\frac{359037739\eta^2}{20901888}+\frac{10647791\eta^3}{2239488}\right.$$
$$+\frac{12091\log(2)}{3780}+\frac{26001\log(3)}{1120}+\left.\frac{3317\log(x)}{504}\right)\chi^{-19/18}+\left(\frac{218158012165}{49161240576}-\frac{34611934451\eta}{1755758592}+\frac{191583143\eta^2}{6967296}\right.$$
$$\left.-\frac{8629979\eta^3}{746496}\right)\chi^{-31/18}-\frac{142129\pi^2}{20736}\chi^{-37/18}+\left(\frac{81733950943}{49161240576}-\frac{6152132057\eta}{1755758592}-\frac{1348031\eta^2}{331776}\right.$$
$$\left.+\frac{6660767\eta^3}{746496}\right)\chi^{-43/18}+\left(\frac{216750571931393}{2703868231680}+\frac{103537\pi^2}{41472}-\frac{3317\gamma}{252}+\left(\frac{866955547}{179159040}-\frac{3977\pi^2}{2304}\right)\eta\right.$$
$$\left.-\frac{130785737\eta^2}{20901888}-\frac{4740155\eta^3}{2239488}-\frac{12091\log(2)}{3780}-\frac{26001\log(3)}{1120}-\frac{3317\log(x)}{504}-\frac{3317\log(\chi)}{756}\right)\chi^{-55/18}, \tag{C4a}$$

$$\mathcal{E}''_6=\left(-\frac{110724557880778937}{704550807797760}+\frac{600535883\pi^2}{75644928}+\frac{11022391\gamma}{459648}+\left(\frac{536131194179051}{16012518359040}+\frac{13215571\pi^2}{4202496}\right)\eta\right.$$
$$\left.-\frac{1193082406697\eta^2}{38125043712}+\frac{35382609493\eta^3}{4084826112}+\frac{40178393\log(2)}{6894720}+\frac{28800441\log(3)}{680960}+\frac{11022391\log(x)}{919296}\right)\chi^{-19/18}$$
$$+\left(\frac{29787660990550865}{1165711336538112}-\frac{591234360321013\eta}{5947506819072}+\frac{107636760191\eta^2}{874119168}-\frac{64940942431\eta^3}{1361608704}\right)\chi^{-31/18}$$
$$-\frac{495811927\pi^2}{18911232}\chi^{-37/18}+\left(\frac{59358100103030627}{8159979355766784}+\frac{2420024232862595\eta}{291427834134528}-\frac{103398129181999\eta^2}{1156459659264}\right.$$
$$\left.+\frac{847423952119\eta^3}{9531260928}\right)\chi^{-43/18}+\left(-\frac{3881667007528080426037}{2243994322835865600}+\frac{720177509\pi^2}{75644928}+\frac{517414657\gamma}{2298240}\right.$$
$$+\left(-\frac{1395931720786001359}{1457139170672640}+\frac{295851449\pi^2}{4202496}\right)\eta-\frac{112681906698415\eta^2}{3469378977792}-\frac{1549239851389\eta^3}{28593782784}$$
$$\left.+\frac{1017275237747\log(2)}{6894720}-\frac{5477465997\log(3)}{680960}+\frac{517414657\log(x)}{4596480}-\frac{517414657\log(\chi)}{6894720}\right)\chi^{-55/18}$$
$$+\left(\frac{152896024020300184249}{67999827964723200}-\frac{95207357\pi^2}{8404992}-\frac{245954159\gamma}{766080}+\left(\frac{12374839994637661}{10793623486464}-\frac{116237911\pi^2}{1400832}\right)\eta\right.$$
$$\left.-\frac{3908281091711\eta^2}{128495517696}-\frac{42680326813\eta^3}{1059028992}-\frac{339627457731\log(2)}{2298240}+\frac{53622642331\log(3)}{680960}-\frac{245954159\log(x)}{1532160}\right)\chi^{-19/6}$$
$$+\left(\frac{23176718595161489}{906664372862976}-\frac{866895029665039\eta}{32380870459392}-\frac{5814138473063\eta^2}{42831839232}+\frac{625202673113\eta^3}{353009664}\right)\chi^{-23/6}+\frac{149592469\pi^2}{2101248}\chi^{-25/6}$$
$$+\left(-\frac{99813874374700537}{234850269265920}-\frac{429547595\pi^2}{8404992}+\frac{11022391\gamma}{153216}+\left(-\frac{62659748948903}{1779168706560}+\frac{13215571\pi^2}{1400832}\right)\eta\right.$$
$$\left.-\frac{95613034561\eta^2}{1412038656}+\frac{22151672941\eta^3}{151289856}+\frac{40178393\log(2)}{2298240}+\frac{86401323\log(3)}{680960}+\frac{11022391\log(x)}{306432}-\frac{11022391\log(\chi)}{459648}\right)\chi^{-31/6}$$
$$+\left(\frac{31472267987495}{6167784849408}-\frac{318662569276073\eta}{4625838637056}+\frac{4844584781833\eta^2}{18356502528}-\frac{1562882519\eta^3}{5603328}\right)\chi^{-9/2}. \tag{C4b}$$

We have pursued careful checking of our results with what is available in Ref. [49] and observed a slight typo in the $\mathcal{O}(e_0^5)$ contributions for the e_t expression [Eq. (A6e) of Ref. [49]]. The η independent term present in the coefficient of $\chi^{-119/18}$ should be $1695261056000 3855/162260186038272$ instead of $16633441088056655/162260186038272$. Note that the above e_t expression is required while computing the Fourier amplitudes ξ_j. Additionally, it is a crucial ingredient while computing the analytic expression for our Fourier phases Ψ_j. It should be obvious that its frequency dependence is encapsulated in $\chi = F/F_0$ and the PN expansion parameter $x = (Gm2\pi F/c^3)^{2/3}$.

We now display our 3PN-accurate closed form expression for the Fourier phases $\Psi_j^{\pm n}$. Recall that *nine* different Fourier phases appear in our 1PN-accurate amplitude-corrected $\tilde{h}(f)$ expression, given by Eq. (3.17). To circumvent the task of displaying all the nine different Fourier phases separately, we provide a general expression for these phases as Ψ_j^n where $n = 0, 1, 2, 3, 4$. It is not very difficult to obtain $\Psi_j^{\pm n}$ from Ψ_j^n by replacing n with the appropriate $'\pm'$ sign in the expression. The general expression for the 3PN-accurate Fourier phase reads

$$\Psi_j^n = (j-(j+n)k_{(3)}^{(6)})\phi_c - 2\pi f t_c - \frac{3j}{256\eta x^{5/2}}\sum_{m=0}^{6}\mathcal{P}_m x^{m/2}. \tag{C5}$$

Various PN coefficients $\mathcal{P}_m$ with next-to-leading order eccentricity contributions are given by

$$\mathcal{P}_0 = 1 - \frac{2355}{1462}e_0^2\chi^{-19/9} + \left(-\frac{2608555}{444448}\chi^{-19/9} + \frac{5222765}{998944}\chi^{-38/9}\right)e_0^4, \tag{C6a}$$

$$\mathcal{P}_1 = 0, \tag{C6b}$$

$$\begin{aligned}\mathcal{P}_2 = &-\frac{2585}{756} - \frac{25n}{3j} + \frac{55\eta}{9} + \left\{\left(\frac{69114725}{14968128} + \frac{1805n}{172j} - \frac{128365\eta}{12432}\right)\chi^{-19/9} + \left(-\frac{2223905}{491232} + \frac{154645\eta}{17544}\right)\chi^{-25/9}\right\}e_0^2 \\ &+ \left\{\left(\frac{229668231175}{13650932736} + \frac{315685n}{8256j} - \frac{426556895\eta}{11337984}\right)\chi^{-19/9} + \left(-\frac{14275935425}{416003328} + \frac{209699405\eta}{4000032}\right)\chi^{-25/9}\right. \\ &+ \left(-\frac{259509826776175}{13976341456896} - \frac{225548425n}{6014496j} + \frac{1222893635\eta}{28804608}\right)\chi^{-38/9} \\ &\left.+ \left(\frac{14796093245}{503467776} - \frac{1028884705\eta}{17980992}\right)\chi^{-44/9}\right\}e_0^4,\end{aligned} \tag{C6c}$$

$$\begin{aligned}\mathcal{P}_3 = &-16\pi + \left(\frac{65561\pi}{4080}\chi^{-19/9} - \frac{295945\pi}{35088}\chi^{-28/9}\right)e_0^2 + \left(\frac{217859203\pi}{3720960}\chi^{-19/9} - \frac{3048212305\pi}{64000512}\chi^{-28/9}\right. \\ &\left.- \frac{6211173025\pi}{102085632}\chi^{-38/9} + \frac{1968982405\pi}{35961984}\chi^{-47/9}\right)e_0^4,\end{aligned} \tag{C6d}$$

$$\begin{aligned}\mathcal{P}_4 = &-\frac{48825515}{508032} - \frac{31805n}{252j} + \left(\frac{22105}{504} - \frac{10n}{j}\right)\eta + \frac{3085\eta^2}{72} + \left\{\left(\frac{115250777195}{2045440512} + \frac{323580365n}{5040288j} + \left(-\frac{72324815665}{6562454976}\right.\right.\right. \\ &\left.\left.+ \frac{36539875n}{1260072j}\right)\eta - \frac{10688155\eta^2}{294624}\right)\chi^{-19/9} + \left(\frac{195802015925}{15087873024} + \frac{5113565n}{173376j} + \left(-\frac{3656612095}{67356576} - \frac{355585n}{6192j}\right)\eta\right. \\ &\left.+ \frac{25287905\eta^2}{447552}\right)\chi^{-25/9} + \left(\frac{936702035}{1485485568} + \frac{3062285\eta}{260064} - \frac{14251675\eta^2}{631584}\right)\chi^{-31/9}\Big\}e_0^2 + \left\{\left(\frac{382978332618985}{1865441746944}\right.\right. \\ &+ \frac{1075257552895n}{4596742656j} + \left(-\frac{240335362454795}{5984958938112} + \frac{121422004625n}{1149185664j}\right)\eta - \frac{35516739065\eta^2}{268697088}\Big)\chi^{-19/9} \\ &+ \left(\frac{1256913822951125}{12777273040896} + \frac{1727660975n}{7727616j} + \left(-\frac{1182697961961875}{3194318260224} - \frac{25377635n}{74304j}\right)\eta + \frac{34290527545\eta^2}{102041856}\right)\chi^{-25/9} \\ &+ \left(-\frac{94372278903235}{7251965779968} + \frac{126823556396665\eta}{733829870592} - \frac{20940952805\eta^2}{93768192}\right)\chi^{-31/9} + \left(-\frac{359074780345285439107}{1705190973672775680}\right. \\ &\left.\left.- \frac{100456187745548465n}{451108723193856j} + \left(-\frac{41964795442387913}{5074973135930880} - \frac{656130734149165n}{3717929037312j}\right)\eta + \frac{203366083643\eta^2}{1130734080}\right)\chi^{-38/9}\right.\end{aligned}$$

$$+\left(-\frac{735191339256903775}{7044076094275584}-\frac{638978688025n}{3031305984j}+\left(\frac{55579511401449335}{125787073112064}+\frac{44433039725n}{108260928j}\right)\eta\right.$$
$$\left.-\frac{240910046095\eta^2}{518482944}\right)\chi^{-44/9}+\left(\frac{3654447011975}{98224939008}-\frac{4300262795285\eta}{18124839936}+\frac{392328884035\eta^2}{1294631424}\right)\chi^{-50/9}\Big\}e_0^4, \tag{C6e}$$

$$\mathcal{P}_5=\frac{14453\pi}{756}-\frac{32\pi n}{j}-\frac{65\pi}{9}\eta-\left(\frac{1675}{756}+\frac{160n}{3j}+\frac{65\eta}{9}\right)\pi\log\left(\frac{f}{j}\right)+\Big\{\Big(-\frac{458370775\pi}{6837264}-\frac{4909969\pi n}{46512j}$$
$$+\frac{15803101\pi\eta}{229824}\Big)\chi^{-19/9}+\left(\frac{185734313\pi}{4112640}-\frac{12915517\pi\eta}{146880}\right)\chi^{-25/9}+\left(\frac{26056251325\pi}{1077705216}+\frac{680485\pi n}{12384j}\right.$$
$$\left.-\frac{48393605\pi\eta}{895104}\right)\chi^{-28/9}+\left(-\frac{7063901\pi}{520128}+\frac{149064749\pi\eta}{2210544}\right)\chi^{-34/9}\Big\}e_0^2+\Big\{\Big(-\frac{1523166085325\pi}{6235584768}$$
$$-\frac{16315826987\pi n}{42418944j}+\frac{52513704623\pi\eta}{209599488}\Big)\chi^{-19/9}+\left(\frac{238457223541\pi}{696563712}-\frac{17513506613\pi\eta}{33488640}\right)\chi^{-25/9}$$
$$+\left(\frac{268377522549925\pi}{1965734313984}+\frac{368891935\pi n}{1188864j}-\frac{498450665645\pi\eta}{1632669696}\right)\chi^{-28/9}+\left(-\frac{2408172473789\pi}{6790791168}\right.$$
$$\left.+\frac{992200223893\pi\eta}{1697697792}\right)\chi^{-34/9}+\left(\frac{34901256494241693175\pi}{79386134731997184}+\frac{84423313781887\pi n}{193345546752j}-\frac{15387742160333\pi\eta}{39404703744}\right)\chi^{-38/9}$$
$$+\left(-\frac{17596253179825\pi}{51451158528}+\frac{1223601085925\pi\eta}{1837541376}\right)\chi^{-44/9}+\left(-\frac{7525784976509075\pi}{38703714803712}-\frac{85031756225\pi n}{216521856j}\right.$$
$$\left.+\frac{461030900395\pi\eta}{1036965888}\right)\chi^{-47/9}+\left(\frac{14896370333\pi}{61544448}-\frac{351697861441\pi\eta}{476969472}\right)\chi^{-53/9}\Big\}e_0^4. \tag{C6f}$$

For the ease of presentation, we split the 3PN contributions to Ψ_j^n into three parts

$$\mathcal{P}_6=\mathcal{P}_6'+\mathcal{P}_6''e_0^2+\mathcal{P}_6'''e_0^4. \tag{C7}$$

Various contributions to $\mathcal{P}_6$ are given by

$$\mathcal{P}_6'=\frac{13966988843531}{4694215680}+\frac{257982425n}{508032j}-\frac{640\pi^2}{3}-\frac{6848\gamma}{21}+\left(-\frac{20562265315}{3048192}-\frac{2393105n}{1512j}+\frac{23575\pi^2}{96}\right.$$
$$\left.+\frac{1845\pi^2 n}{32j}\right)\eta+\left(\frac{110255}{1728}+\frac{475n}{24j}\right)\eta^2-\frac{127825\eta^3}{1296}-\frac{13696\log(2)}{21}-\frac{3424\log(x)}{21}, \tag{C8a}$$

$$\mathcal{P}_6''=\Big\{\frac{4175723876720788380517}{5556561877278720000}+\frac{534109712725265n}{2405438042112j}-\frac{21508213\pi^2}{276480}-\frac{734341\gamma}{16800}+\Big(-\frac{37399145056383727}{28865256505344}$$
$$-\frac{1219797059185n}{2045440512j}+\frac{12111605\pi^2}{264192}+\frac{639805n\pi^2}{22016j}\Big)\eta+\left(-\frac{159596464273381}{1718170030080}+\frac{43766986495n}{1022720256j}\right)\eta^2-\frac{69237581\eta^3}{746496}$$
$$-\frac{9663919\log(2)}{50400}+\frac{4602177\log(3)}{44800}-\frac{734341\log(x)}{33600}\Big\}\chi^{-19/9}+\Big\{\frac{326505451793435}{2061804036096}+\frac{916703174045n}{5080610304j}$$
$$-\left(\frac{13467050491570355}{39689727694848}+\frac{9519440485n}{35282016j}\right)\eta-\left(\frac{2186530635995}{52499639808}+\frac{7198355375n}{45362592j}\right)\eta^2+\frac{2105566535\eta^3}{10606464}\Big\}\chi^{-25/9}$$
$$+\frac{24716497\pi^2}{293760}\chi^{-28/9}+\Big\{-\frac{82471214720975}{45625728024576}-\frac{2153818055n}{524289024j}+\left(-\frac{48415393035455}{1629490286592}-\frac{119702185n}{1560384j}\right)\eta$$

$$+\left(\frac{906325428545}{6466231296}+\frac{32769775n}{222912j}\right)\eta^2-\frac{2330466575\eta^3}{16111872}\Big\}\chi^{-31/9}+\Big\{-\frac{4165508390854487}{16471063977984}-\frac{96423905\pi^2}{5052672}$$
$$+\frac{2603845\gamma}{61404}+\left(-\frac{1437364085977}{53477480448}+\frac{3121945\pi^2}{561408}\right)\eta+\frac{4499991305\eta^2}{636636672}+\frac{2425890995\eta^3}{68211072}+\frac{1898287\log(2)}{184212}$$
$$+\frac{12246471\log(3)}{163744}+\frac{2603845\log(x)}{122808}-\frac{2603845\log(\chi)}{184212}\Big\}\chi^{-37/9}, \tag{C8b}$$

$$\mathcal{P}_6'''=\Big\{\frac{13875930442343179788457991}{5067584432078192640000}+\frac{1774846575386055595n}{2193759494406144j}-\frac{71471791799\pi^2}{252149760}-\frac{2440215143\gamma}{15321600}$$
$$+\left(-\frac{124277359022363124821}{26325113932873728}-\frac{4053385627671755n}{1865441746944j}+\frac{40246863415\pi^2}{240943104}+\frac{2126072015n\pi^2}{20078592j}\right)\eta$$
$$+\left(-\frac{530339050780445063}{1566971067432960}+\frac{7654615585415n}{49090572288j}\right)\eta^2-\frac{230076481663\eta^3}{680804352}-\frac{32113202837\log(2)}{45964800}$$
$$+\frac{5097678057\log(3)}{13619200}-\frac{2440215143\log(x)}{30643200}\Big\}\chi^{-19/9}+\Big\{\frac{2095939685244436475}{1746053475139584}+\frac{5884601777755325n}{4302551126016j}$$
$$+\left(-\frac{17381974915387486205}{8402882349109248}-\frac{527634379756765n}{358545927168j}\right)\eta+\left(-\frac{386694251193132845}{933653594345472}-\frac{9761006428375n}{10342670976j}\right)\eta^2$$
$$+\frac{2855158909615\eta^3}{2418273792}\Big\}\chi^{-25/9}+\frac{254578148953\pi^2}{535818240}\chi^{-28/9}+\Big\{\frac{141251897794072110575}{3786570420215611392}+\frac{194154433667165n}{2290094456832j}$$
$$+\left(-\frac{11182467092862313645}{19319236837834752}-\frac{15348073704055n}{13631514624j}\right)\eta+\left(\frac{1038816664853665}{594291769344}+\frac{2534255435n}{1741824j}\right)\eta^2$$
$$-\frac{147245442666235\eta^3}{102858190848}\Big\}\chi^{-31/9}+\Big\{\frac{102453749612934666311}{19868699733442560}-\frac{598067688595\pi^2}{4608036864}-\frac{36290762107\gamma}{56000448}$$
$$+\left(\frac{6738669506224179365}{2219101528670208}-\frac{110934582115\pi^2}{512004096}\right)\eta-\frac{1484623162301215\eta^2}{6604468835328}+\frac{128895671353745\eta^3}{217729741824}$$
$$-\frac{1140350944327\log(2)}{24000192}+\frac{1296725746149\log(3)}{49778176}-\frac{36290762107\log(x)}{112000896}+\frac{36290762107\log(\chi)}{168001344}\Big\}\chi^{-37/9}$$
$$+\Big\{-\frac{31234883302860809055617197 73}{35508564115571895828480 0}-\frac{8528066087750623810 7n}{124770071244349440j}+\frac{300051120571\pi^2}{970776576}+\frac{211649317\gamma}{191520}$$
$$+\left(-\frac{40336854286157147692937}{32939298808508252160}+\frac{584462420500316711n}{495119330334720j}+\frac{2786391039419\pi^2}{17972849664}-\frac{91683875075n\pi^2}{1089263616j}\right)\eta$$
$$+\left(\frac{14654969487690651143}{35648591784099840}-\frac{46042929781519n}{107385626880j}\right)\eta^2+\frac{49171400252465\eta^3}{91738386432}+\frac{2117998887803\log(2)}{44241120}$$
$$-\frac{334711679031\log(3)}{13108480}+\frac{211649317\log(x)}{383040}\Big\}\chi^{-38/9}+\Big\{-\frac{1017258852718193648990131}{859416250731078942720}$$
$$-\frac{2845923798831388013 45n}{227358796489703424j}+\left(\frac{6931109654216181201 3731}{30693437526109962240}+\frac{176024840748197725 15n}{12179935526234112j}\right)\eta$$
$$+\left(\frac{3272123415010135297}{2970715982008320}+\frac{129257754627385505n}{66922722671616j}\right)\eta^2-\frac{400631184776 71\eta^3}{20353213440}\Big\}\chi^{-44/9}$$
$$-\frac{2341612230425\pi^2}{3675082752}\chi^{-47/9}+\Big\{-\frac{1815829184426912901 25}{1374276523167055872}-\frac{157819616198875n}{591398019072j}+\Big(\frac{1741702918744309017425}{1521520436363526144}$$
$$+\frac{185709581143825n}{109127015424j}\Big)\eta+\left(-\frac{18130335399490218365}{6037779509379072}-\frac{16942972137575n}{7794786816j}\right)\eta^2+\frac{91862546967565\eta^3}{37330771968}\Big\}\chi^{-50/9}$$

$$+\left\{\frac{259620437372696563}{159257838845952}+\frac{6919171299\pi^2}{2589262848}-\frac{558835855\gamma}{2030112}+\left(-\frac{245999063921173}{13702378991616}-\frac{20770936405\pi^2}{575391744}\right)\eta\right.$$
$$+\frac{255806950720535\eta^2}{326247118848}-\frac{9022269087085\eta^3}{8738762112}-\frac{12629690323\log(2)}{188800416}-\frac{27159422553\log(3)}{55940864}-\frac{558835855\log(x)}{4060224}$$
$$\left.+\frac{558835855\log(\chi)}{6090336}\right\}\chi^{-56/9}. \tag{C8c}$$

Let us emphasize that the above expression indeed provides all the required Fourier phases, $\Psi_j^{\pm n}$'s that appear in Eq. (3.17) for $\tilde{h}(f)$. For instance, Fourier phases present in the quadrupolar-order $\tilde{h}(f)$, namely, Ψ_j^0, Ψ_j^{+2}, and Ψ_j^{-2} are obtained by putting in Eq. (C5) $n=0,+2,-2$, respectively. Further, one should evaluate these Fourier phases at the correct stationary points and this requires us to use $x=\{\frac{Gm2\pi f}{c^3(j-(j\pm n)k_{(3)}^{(6)})}\}^{2/3}$. We note in passing that the 3PN-accurate e_t and Ψ_j^n expressions along with the 1PN-accurate Fourier amplitudes while incorporating eccentricity corrections to $\mathcal{O}(e_0^6)$ at each PN order can be found in the attached Mathematica notebook [65].

[1] B. P. Abbott, R. Abbott, T. D. Abbott, M. R. Abernathy, F. Acernese, K. Ackley, C. Adams, T. Adams, P. Addesso, R. X. Adhikari *et al.*, Phys. Rev. Lett. **116**, 131103 (2016).
[2] F. Acernese, M. Agathos, K. Agatsuma, D. Aisa, N. Allemandou, A. Allocca, J. Amarni, P. Astone, G. Balestri, G. Ballardin *et al.*, Classical Quantum Gravity **32**, 024001 (2015).
[3] B. P. Abbott, R. Abbott, T. D. Abbott, M. R. Abernathy, F. Acernese, K. Ackley, C. Adams, T. Adams, P. Addesso, R. X. Adhikari *et al.*, Phys. Rev. Lett. **116**, 061102 (2016).
[4] B. P. Abbott, R. Abbott, T. D. Abbott, M. R. Abernathy, F. Acernese, K. Ackley, C. Adams, T. Adams, P. Addesso, R. X. Adhikari *et al.*, Phys. Rev. Lett. **116**, 241103 (2016).
[5] B. P. Abbott, R. Abbott, T. D. Abbott, F. Acernese, K. Ackley, C. Adams, T. Adams, P. Addesso, R. X. Adhikari, V. B. Adya *et al.*, Phys. Rev. Lett. **118**, 221101 (2017).
[6] B. P. Abbott, R. Abbott, T. D. Abbott, F. Acernese, K. Ackley, C. Adams, T. Adams, P. Addesso, R. X. Adhikari, V. B. Adya *et al.*, Astrophys. J. Lett. **851**, L35 (2017).
[7] B. P. Abbott, R. Abbott, T. D. Abbott, F. Acernese, K. Ackley, C. Adams, T. Adams, P. Addesso, R. X. Adhikari, V. B. Adya *et al.*, Phys. Rev. Lett. **119**, 141101 (2017).
[8] B. P. Abbott, R. Abbott, T. D. Abbott, F. Acernese, K. Ackley, C. Adams, T. Adams, P. Addesso, R. X. Adhikari, V. B. Adya *et al.*, Phys. Rev. Lett. **119**, 161101 (2017).
[9] LIGO Scientific and Virgo Collaborations, arXiv:1811.12907.
[10] K. Belczynski, D. E. Holz, T. Bulik, and R. O'Shaughnessy, Nature (London) **534**, 512 (2016).
[11] D. Park, C. Kim, H. M. Lee, Y.-B. Bae, and K. Belczynski, Mon. Not. R. Astron. Soc. **469**, 4665 (2017).
[12] B.-M. Hoang, S. Naoz, B. Kocsis, F. A. Rasio, and F. Dosopoulou, Astrophys. J. **856**, 140 (2018).
[13] B. McKernan, K. E. S. Ford, J. Bellovary, N. W. C. Leigh, Z. Haiman, B. Kocsis, W. Lyra, M.-M. Mac Low, B. Metzger, M. O'Dowd *et al.*, Astrophys. J. **866**, 66 (2018).
[14] K. Kremer, S. Chatterjee, K. Breivik, C. L. Rodriguez, S. L. Larson, and F. A. Rasio, Phys. Rev. Lett. **120**, 191103 (2018).
[15] C. L. Rodriguez, M. Zevin, C. Pankow, V. Kalogera, and F. A. Rasio, Astrophys. J. Lett. **832**, L2 (2016).
[16] X. Chen and P. Amaro-Seoane, Astrophys. J. Lett. **842**, L2 (2017).
[17] A. Nishizawa, A. Sesana, E. Berti, and A. Klein, Mon. Not. R. Astron. Soc. **465**, 4375 (2017).
[18] B. P. Abbott, R. Abbott, T. D. Abbott, M. R. Abernathy, F. Acernese, K. Ackley, C. Adams, T. Adams, P. Addesso, R. X. Adhikari *et al.*, Phys. Rev. Lett. **116**, 241102 (2016).
[19] E. A. Huerta, P. Kumar, B. Agarwal, D. George, H.-Y. Schive, H. P. Pfeiffer, R. Haas, W. Ren, T. Chu, M. Boyle *et al.*, Phys. Rev. D **95**, 024038 (2017).
[20] C. L. Rodriguez, S. Chatterjee, and F. A. Rasio, Phys. Rev. D **93**, 084029 (2016).
[21] J. Samsing, M. MacLeod, and E. Ramirez-Ruiz, Astrophys. J. **784**, 71 (2014).
[22] J. Samsing and E. Ramirez-Ruiz, Astrophys. J. **840**, L14 (2017).
[23] C. L. Rodriguez, P. Amaro-Seoane, S. Chatterjee, and F. A. Rasio, Phys. Rev. Lett. **120**, 151101 (2018).
[24] J. Samsing, Phys. Rev. D **97**, 103014 (2018).
[25] C. L. Rodriguez, P. Amaro-Seoane, S. Chatterjee, K. Kremer, F. A. Rasio, J. Samsing, C. S. Ye, and M. Zevin, Phys. Rev. D **98**, 123005 (2018).
[26] R. M. OLeary, Y. Meiron, and B. Kocsis, Astrophys. J. Lett. **824**, L12 (2016).
[27] L. Randall and Z.-Z. Xianyu, Astrophys. J. **864**, 134 (2018).
[28] M. Zevin, J. Samsing, C. Rodriguez, C.-J. Haster, and E. Ramirez-Ruiz, Astrophys. J. **871**, 91 (2019).
[29] L. Gondán, B. Kocsis, P. Raffai, and Z. Frei, Astrophys. J. **855**, 34 (2018).
[30] L. Gondán and B. Kocsis, Astrophys. J. **871**, 178 (2019).

[31] S. Burke-Spolaor, S. R. Taylor, M. Charisi, T. Dolch, J. S. Hazboun, A. M. Holgado, L. Z. Kelley, T. J. W. Lazio, D. R. Madison, N. McMann *et al.*, arXiv:1811.08826.

[32] M. Bonetti, A. Sesana, F. Haardt, E. Barausse, and M. Colpi, Mon. Not. R. Astron. Soc. **486**, 4044 (2019).

[33] I. Hinder, F. Herrmann, P. Laguna, and D. Shoemaker, Phys. Rev. D **82**, 024033 (2010).

[34] T. Damour, A. Gopakumar, and B. R. Iyer, Phys. Rev. D **70**, 064028 (2004).

[35] C. Königsdörffer and A. Gopakumar, Phys. Rev. D **73**, 124012 (2006).

[36] I. Hinder, L. E. Kidder, and H. P. Pfeiffer, Phys. Rev. D **98**, 044015 (2018).

[37] E. A. Huerta, C. J. Moore, P. Kumar, D. George, A. J. K. Chua, R. Haas, E. Wessel, D. Johnson, D. Glennon, A. Rebei *et al.*, Phys. Rev. D **97**, 024031 (2018).

[38] T. Damour and A. Nagar, in *Lecture Notes in Physics*, edited by F. Haardt, V. Gorini, U. Moschella, A. Treves, and M. Colpi (Springer Verlag, Berlin, 2016), Vol. 905, p. 273.

[39] T. Hinderer and S. Babak, Phys. Rev. D **96**, 104048 (2017).

[40] Z. Cao and W.-B. Han, Phys. Rev. D **96**, 044028 (2017).

[41] W. E. East, S. T. McWilliams, J. Levin, and F. Pretorius, Phys. Rev. D **87**, 043004 (2013).

[42] V. Tiwari, S. Klimenko, N. Christensen, E. A. Huerta, S. R. P. Mohapatra, A. Gopakumar, M. Haney, P. Ajith, S. T. McWilliams, G. Vedovato *et al.*, Phys. Rev. D **93**, 043007 (2016).

[43] A. Buonanno, B. R. Iyer, E. Ochsner, Y. Pan, and B. S. Sathyaprakash, Phys. Rev. D **80**, 084043 (2009).

[44] N. Yunes, K. G. Arun, E. Berti, and C. M. Will, Phys. Rev. D **80**, 084001 (2009).

[45] Y. Boetzel, A. Susobhanan, A. Gopakumar, A. Klein, and P. Jetzer, Phys. Rev. D **96**, 044011 (2017).

[46] M. Tessmer and A. Gopakumar, Mon. Not. R. Astron. Soc. **374**, 721 (2007).

[47] R.-M. Memmesheimer, A. Gopakumar, and G. Schäfer, Phys. Rev. D **70**, 104011 (2004).

[48] A. Królak, K. D. Kokkotas, and G. Schäfer, Phys. Rev. D **52**, 2089 (1995).

[49] S. Tanay, M. Haney, and A. Gopakumar, Phys. Rev. D **93**, 064031 (2016).

[50] K. G. Arun, L. Blanchet, B. R. Iyer, and S. Sinha, Phys. Rev. D **80**, 124018 (2009).

[51] A. Klein, Y. Boetzel, A. Gopakumar, P. Jetzer, and L. de Vittori, Phys. Rev. D **98**, 104043 (2018).

[52] T. Damour, B. R. Iyer, and B. S. Sathyaprakash, Phys. Rev. D **57**, 885 (1998).

[53] K. S. Thorne, *300 years of Gravitation*, edited by S. W. Hawking and W. Israel (Cambridge University press, Cambridge, 1989), pp. 330–458.

[54] P. Colwell, *Solving Kepler's Equation Over Three Centuries* (Willmann-Bell, Richmond, VA, 1993).

[55] P. C. Peters and J. Mathews, Phys. Rev. **131**, 435 (1963).

[56] P. C. Peters, Phys. Rev. **136**, B1224 (1964).

[57] W. Junker and G. Schaefer, Mon. Not. R. Astron. Soc. **254**, 146 (1992).

[58] B. Moore, T. Robson, N. Loutrel, and N. Yunes, Classical Quantum Gravity **35**, 235006 (2018).

[59] B. Mikóczi, B. Kocsis, P. Forgács, and M. Vasúth, Phys. Rev. D **86**, 104027 (2012).

[60] V. Pierro, I. M. Pinto, and A. D. A. M. Spallicci di F., Mon. Not. R. Astron. Soc. **334**, 855 (2002).

[61] V. Pierro, I. Pinto, A. Spallicci, E. Laserra, and F. Recano, Mon. Not. R. Astron. Soc. **325**, 358 (2001).

[62] C. M. Bender and S. A. Orszag, *Advanced Mathematical Methods for Scientists and Engineers* (Springer, New York, 1999).

[63] B. Moore, M. Favata, K. G. Arun, and C. K. Mishra, Phys. Rev. D **93**, 124061 (2016).

[64] L. Blanchet, T. Damour, and B. R. Iyer, Phys. Rev. D **51**, 5360 (1995).

[65] See Supplemental Material at http://link.aps.org/supplemental/10.1103/PhysRevD.99.124008, for extracting our fully analytic expression of 1PN amplitude-corrected $\tilde{h}(f)$ with advance of periastron incorporated (3.17). It also contains complete analytic expressions for 3PN-accurate e_t and Fourier phases Ψ_j^n that includes effect of periastron advance (These expressions are already listed in Appendix C but only upto next-to leading order in e_0). The Γ and Σ coefficients in Appendix A can also be obtained from this notebook.

[66] L. Blanchet, B. R. Iyer, C. M. Will, and A. G. Wiseman, Classical Quantum Gravity **13**, 575 (1996).

[67] C. Moreno-Garrido, J. Buitrago, and E. Mediavilla, Mon. Not. R. Astron. Soc. **266**, 16 (1994).

[68] E. Mediavilla, J. Buitrago, and C. Moreno-Garrido, Mon. Not. R. Astron. Soc. **274**, 115 (1995).

[69] G. M. Harry and LIGO Scientific Collaboration, Classical Quantum Gravity **27**, 084006 (2010).

[70] A. Nitz, I. Harry, D. Brown, C. M. Biwer, J. Willis, T. D. Canton, L. Pekowsky, C. Capano, T. Dent, A. R. Williamson *et al.*, gwastro/pycbc: Pre-o3 release v1, 2019, https://doi.org/10.5281/zenodo.2556644.

[71] J. D. E. Creighton and W. G. Anderson, *Gravitational-Wave Physics and Astronomy: An Introduction to Theory, Experiment and Data Analysis* (Wiley-VCH, Weinheim, 2011).

[72] C. Van Den Broeck and A. S. Sengupta, Classical Quantum Gravity **24**, 155 (2007).

[73] C. Königsdörffer and A. Gopakumar, Phys. Rev. D **71**, 024039 (2005).

[74] L. E. Kidder, Phys. Rev. D **52**, 821 (1995).

[75] N. Seto, Phys. Rev. Lett. **87**, 251101 (2001).

[76] A. H. Mroué, H. P. Pfeiffer, L. E. Kidder, and S. A. Teukolsky, Phys. Rev. D **82**, 124016 (2010).

[77] B. Moore and N. Yunes, arXiv:1903.05203.

[78] J. D. Hunter, Comput. Sci. Eng. **9**, 90 (2007).